

The Luminosity Function of Star Clusters in 20 Star-Forming Galaxies Based on Hubble Legacy Archive Photometry¹

BRADLEY C. WHITMORE², RUPALI CHANDAR³, ARIEL S. BOWERS^{2,4}, SOEREN LARSEN⁵, KEVIN LINDSAY², ASNA ANSARI^{2,6}, JESSICA EVANS⁷

email: whitmore@stsci.edu, etc

ABSTRACT

Luminosity functions have been determined for star cluster populations in 20 nearby (4–30 Mpc), star-forming galaxies based on ACS source lists generated by the Hubble Legacy Archive. These cluster catalogs provide one of the largest sets of uniform, automatically-generated cluster candidates available in the literature at present. Comparisons are made with other recently generated cluster catalogs demonstrating that the HLA-generated catalogs are of similar quality, but in general do not go as deep. A typical cluster luminosity function can be approximated by a power-law, $dN/dL \propto L^\alpha$, with an average value for α of -2.37 and RMS scatter = 0.18 when using the F814W (“I”) band. A comparison of fitting results based on methods which use binned and unbinned data shows good agreement, although there may be a systematic tendency for the unbinned (maximum likelihood) method to give slightly more negative values of α

¹Based on observations with the NASA/ESA *Hubble Space Telescope*, obtained at the Space Telescope Science Institute, which is operated by the Association of Universities for Research in Astronomy, Inc. under NASA contract NAS5-26555. Also based on data obtained from the Hubble Legacy Archive, which is a collaboration between the Space Telescope Science Institute (STScI/NASA), the Space Telescope European Coordinating Facility (ST-ECF/ESA) and the Canadian Astronomy Data Centre (CADC/NRC/CSA). Support for Program number 11781 was provided by NASA through a grant from the Space Telescope Science Institute.

²Space Telescope Science Institute, 3700 San Martin Drive, Baltimore, Maryland 21218, USA

³University of Toledo, Department of Physics & Astronomy, Toledo, OH 43606, USA

⁴Johns Hopkins University, Baltimore, MD, 21218

⁵Department of Astrophysics/IMAPP, Radboud University Nijmegen, P. O. Box 9010, 6500 GL Nijmegen, The Netherlands

⁶Northwestern University, Evanston, IL, 60201

⁷Univeristy of Illinois, Champaign, IL, 61820

for galaxies with steeper luminosity functions. We find that galaxies with high rates of star formation (or equivalently, with the brightest or largest numbers of clusters) have a slight tendency to have shallower values of α . In particular, the Antennae galaxy (NGC 4038/39), a merging system with a relatively high star formation rate, has the second flattest luminosity function in the sample. A tentative correlation may also be present between Hubble Type and values of α , in the sense that later type galaxies (i.e., Sd and Sm) appear to have flatter luminosity functions. Hence, while there do appear to be some weak correlations, the relative similarity in the values of α for a large number of star-forming galaxies suggests that, to first order, the LFs are fairly universal. We examine the bright end of the luminosity functions and find evidence for a downturn, although it only pertains to about 1% of the clusters. Our uniform database results in a small scatter (≈ 0.4 to 0.5 mag) in the correlation between the magnitude of the brightest cluster ($M_{\text{brightest}}$) and log of the number of clusters brighter than $M_I = -9$ (log N). We also examine the magnitude of the brightest cluster vs. log SFR for a sample including both dwarfs galaxies and ULIRGS. This shows that the correlation extends over roughly six orders of magnitudes but with scatter that is larger than for our spiral sample, probably because of the high levels of extinction in many of the LIRG galaxies.

Subject headings: galaxies: star clusters—galaxies: interactions—galaxies: individual (NGC 45 – NGC 406 – NGC 628 – NGC 1300 – NGC 1309 – NGC 1313 – NGC 1483 – NGC 2397 – NGC 3627 – NGC 4038/39 – NGC 4258 – NGC 4394 – NGC 4395 – NGC 4736 – NGC 5055 – NGC 5236 – NGC 5457 – NGC 6217 – NGC 6503 – NGC 7793)

1. Introduction

Luminosity functions (LFs) provide a basic parameterization of the star cluster population in galaxies. While the cluster mass function is more fundamental, in many cases the multi-wavelength data necessary to age-date the cluster population, and hence determine the cluster masses, does not exist. In addition, the LF is directly observable and does not require the use of a stellar population model that is inherently uncertain. To the degree that the star formation history of different galaxies are similar, the luminosity function can serve as an approximate proxy for the mass function. Some recent questions being addressed using LFs include: 1) how uniform are cluster luminosity functions and what properties do they correlate with (e.g., with star formation history?), 2) what is the shape of the LF and

is there evidence of a change of slope at either the faint or bright end, 3) can the brightest cluster (hereafter $M_{\text{brightest}}$) vs. $\log N$ (number of clusters brighter than $M_I = -9$) relation be described as a single power law with a scatter which is only statistical in nature? Progress answering these questions is hampered by non-uniformity in both the available observational datasets and the criteria used to select clusters. In this paper we provide a large, uniform (Hubble observations using the Advanced Camera for Surveys [ACS]), and automatically-generated (Hubble Legacy Archive [HLA]) database to better address these and other related questions.

The current paper is part of a larger project that aims to detect star clusters in several hundred galaxies using HST imaging. In this first paper, we outline the basic steps used in the determination of luminosity functions for 20 of the galaxies with the highest quality data. We pay particular attention to the selection of the clusters, making comparisons with other recently generated cluster catalogs in order to estimate the degree to which selection effects can impact the results.

This paper is organized as follows. Section 2 describes the initial source lists created by the Hubble Legacy Archive. Section 3 describes some additional processing, and the method used to select the clusters. Section 4 presents the luminosity functions for the target galaxies, including coadditions of galaxies with similar properties (i.e., “super galaxies”), and Section 5 discusses a variety of correlations and their implications. Finally, we summarize our main results in Section 6. The photometric catalogs used in this study are available at <http://archive.stsci.edu/prepds/starclust-sfgal/>.

2. Initial Source Lists from the Hubble Legacy Archive (HLA)

In recent years, star cluster luminosity functions have been determined for a relatively large number of individual galaxies using a wide range of observational setups and selection criteria. However, combining these different studies in an attempt to determine general correlations is problematic due to this diversity (see Portegies Zwart et al. 2010 for a recent discussion).

A primary goal of the current project is to select star clusters in 20 nearby star-forming galaxies in a *homogeneous* and *objective* manner. We only use observations taken with the ACS on the Hubble Space Telescope and employ DAOPHOT-based source lists from the Hubble Legacy Archive (HLA; available at <http://hla.stsci.edu>).

Below, we summarize the basic techniques used to develop the HLA source lists, and refer interested readers to: <http://hla.stsci.edu/hla-faq.html#Source1> for more details.

When available, the HLA combines multiple images from different filters in a visit into a single image to form a “detection” image (also known as a “total” or “white light” image). This technique allows detection of fainter sources with a wider range in colors and ages than observations taken in a single filter, and provides a master file with matched source positions in each filter. A disadvantage is that the completeness thresholds are not uniform for any given filter.

The HLA provides two source lists; one based on DAOPHOT (Stetson 1987) for stars and compact objects and one based on SExtractor (Bertin 1996) for extended objects. This paper is based on the DAOPHOT HLA catalogs, since we are interested in objects that are slightly broader than the PSF (i.e., compact clusters), for galaxies observed using ACS. These catalogs use the routine DAOFIND on median-divided images (see Miller et al. 1999 for a discussion of this technique) to eliminate common problems related to detecting objects in regions of bright and variable local backgrounds, for example, in the high background areas near the center of a spiral galaxy.

The measurements are made by performing circular aperture photometry using the DAOPHOT/PHOT package/task in IRAF with a 3 pixel ($0.15''$) radius and the ABMAG photometric system. For consistency with most previous work in this field, we prefer to use the VEGAMAG system. We therefore convert the photometry provided by the HLA on the ABMAG system to the VEGAMAG system using Table 10 from Sirianni et al. (2005) for ACS.

3. Additional Processing and Selection of the Clusters

3.1. Galaxy Sample

In this paper, we select 20 star-forming galaxies with some of the highest quality ACS multi-wavelength observations available. The galaxies and observations satisfy the following criteria: (1) distance modulus $m - M \lesssim 32$ (i.e., distance $\lesssim 30$ Mpc) (2) galaxy type of Sa or later; (3) images taken with the Wide Field Camera of ACS in the F814W ($\approx I$ band) and at least one other broad-band optical filter, preferably a V band filter; (4) source lists exist in the HLA as of October 2010, and reach to at least $M_I \approx -9$.

The sample galaxies are listed in Table 1, along with some of their basic properties. These include name, galaxy type, distance modulus, foreground extinction, absolute magnitude M_B , proposal ID and visit, and a list of the ACS filters available for each galaxy (note: WFPC2 F336W observations are also included in italics as reference information, but are not used in the current paper). We also provide an estimate of the star formation rate within

the observed ACS field for each galaxy, as described in Section 3.5.

Color images of the galaxies and the nine brightest clusters are shown in Figure 1.

3.2. Cluster Selection

The selection of star clusters from observations that contain individual stars (both foreground and within the target galaxy), background galaxies, clusters and associations, is one of the most important steps for studies of extragalactic cluster systems. In principle, an objective, completely automated technique would be preferred, especially for large datasets and samples of many galaxies, such as in the current study. However, a combination of potential problems, ranging from crowding to dimming of clusters with age, make this approach problematic. For this reason, many authors use both (or a combination of) automatic and manual techniques (e.g., Chandar et al. 2010, Bastian et al. 2012, Johnson et al. 2012). This is especially appropriate for detailed studies of individual galaxies where the goal is to push to the faintest levels.

For the present study, the approach is to examine cluster luminosity functions, and in the future, mass functions, for a large homogenous sample of galaxies. This requires primarily an automatic approach. One of the difficulties resulting from this approach is the selection of faint clusters without including large numbers of contaminants, such as close pairs of stars. Because of this problem, the limiting magnitudes from this study are brighter than are typically found for detailed studies of cluster systems in individual galaxies. The present paper should therefore be viewed as being complementary to many of the current papers which study the star clusters in nearby galaxies in more detail. Its strength is that it is large, homogeneous, and objective; its weakness is that it can not go as faint as more focussed studies of single galaxies.

While our general approach is to rely on automated selection for the vast majority of the cluster candidates, a manual examination is made for the brightest 10 clusters in each galaxy, since many of the science goals of our project are focussed on these clusters (i.e., the $M_{\text{brightest}}$ vs. log SFR diagram and the possible turnover at the bright end of the luminosity function). Automatic and manual techniques have been compared in various studies (e.g., Chandar et al. 2010; Bastian et al. 2012; Johnson et al. 2012; Chandar et al. 2014). While selection effects are always a concern, results based on different cluster catalogs are usually quite similar (e.g., Chandar et al. 2010 find differences at approximately the 0.1 level when determining values of α using a wide variety of selection criteria). We revisit this question in Section 3.3 with similar results.

Examples of common contaminants found in the catalogs when manually checking the 10 brightest clusters are: 1) bright (saturated) foreground stars, 2) the nucleus of the galaxy, and 3) the presence of bright background galaxies.

The primary diagnostic used for separating stars from clusters in an image is whether the object has the same brightness profile as a star (i.e., the point spread function). In the current paper we follow the general approach used in earlier papers (e.g., Whitmore et al. 2010). We first select training sets of stars and obvious isolated clusters in each target galaxy. These training sets help us determine the best range in values of the concentration index, C (defined as the difference in aperture magnitudes determined using a 3 pix and a 1 pix radius for the HLA) for separating stars from clusters.

In this study, as also found in Chandar et al. (2010), a cut in C alone is not sufficient to separate close pairs of individual stars in the most crowded star-forming regions. In these regions, the concentration index of individual or close blends of stars can be overestimated, thereby raising the C value for non-clusters above the star/cluster cutoff. This problem is greatest in images of nearby galaxies, where the DAOPHOT catalogs can contain large numbers of individual stars detected within a single, highly resolved star cluster. We are able to eliminate most of these contaminants by selecting the brightest object with a C value above our cut and then removing any fainter candidate sources within a radius of R_{neighbor} (typically with values in the range 10–20 pixels—depending primarily on the distance of the galaxy). The program used to make this determination is called UNIQPOS. While this “neighbor removal” step occasionally removes another real cluster nearby, the vast majority of the removed objects are close pairs of stars rather than bona fide compact star clusters. The final values of C and R_{neighbor} applied to the source lists in each galaxy are compiled in Table 2.

We determine the optimal depth of each catalog based on the quality of the observations for each galaxy separately. To accomplish this, we trade depth, and hence size of the catalog, with the fraction of contaminants, which increases at fainter magnitudes. We aim for contamination rates less than 10–20%. A spot check described in Section 5.2 for NGC 1300 and NGC 5457 finds contamination rates in the range 5 to 12%, compatible with our goal. The limiting magnitude used for our cluster samples are primarily driven by the distance of the host galaxy, but there are other factors, such as crowding, exposure time, dithering strategy, etc. that can also affect this limit.

We use a simple prescription to determine aperture corrections, (which converts the fixed 3-pixel radius aperture magnitudes from the HLA to total magnitudes) for our clusters. In general, we determine the mean aperture correction from 3 to 10 pixels (0.5”) based on DAOPHOT measurements for the ten brightest clusters. Clusters are removed from the

determination if a manual examination shows them to be in a very crowded region. An additional correction of 0.10 mag is used to extrapolate from $0.5''$ to infinity, following the procedure in Holtzman et al. (1995).

A weakness of this approach is that by adopting a single value of the aperture correction for all clusters, we overestimate the total luminosity of very compact clusters and underestimate the total luminosity of more extended clusters. Hence, another method that could be used would be to apply aperture corrections to each object based on its measured value of C . In Chandar et al. (2010), we compared the luminosity function of clusters in M83 that result when an average correction is applied to each cluster, versus if a size-dependent aperture correction is applied to each cluster. We find that the method used to determine aperture corrections affect the measurement of α at only the ≈ 0.01 mag level in this particular case.

In the current paper, we also investigate the effect on our results if we use a larger aperture (i.e., a 7 pixel radius with a background sky annulus from 15 to 20 pixels), minimizing the need for an aperture correction. This captures a much larger fraction of the total light from a cluster, at the expense of occasionally including nearby objects in the aperture. Typical differences between the 3 and 7 pixel radii are ≈ 0.7 mag, with scatter of about 0.4 mag. We use an upper limit of 1.5 mag for the difference to guard against outliers (i.e., bright nearby stars within 7 pixels). These are relatively rare, but it is important to remove them since they can cause very large apparent aperture corrections (i.e., up to 4 mag) in some cases. As will be discussed in Sections 5.1 and 5.3, it is reassuring to find that the difference between the use of 3 and 7 pixel apertures introduces relatively minor effects on our results.

Finally, we correct each cluster for foreground extinction (listed in Table 1). We do not, however, correct the luminosities for any extinction within the host galaxy itself. This would only be possible for a few galaxies in the current dataset due to the lack of U band photometry necessary to determine age, mass, and extinction for individual clusters (e.g., see Chandar et al. 2010). However, we note that in Section 5.1 we find that the RMS scatter in the $M_{\text{brightest}}$ vs. $\log N$ and $M_{\text{brightest}}$ vs. $\log \text{SFR}$ relations is only about 0.4 mag, leaving very little room for large values of extinction. Hence extinction is not likely to significantly affect our results. This is not the case for all galaxies, however. For example, in Section 5.3 it is shown that ULIRG galaxies can have much larger values of extinction, dramatically increasing the scatter in the $M_{\text{brightest}}$ vs. $\log N$ diagram.

In Table 2 we list the brightness limits adopted for each cluster catalog, the values of C and R_{neighbor} used to construct the catalogs, magnitude of the brightest cluster in the I band $M_{\text{brightest}}$, and $\log N$ (i.e., \log of the total number of clusters brighter than $M_I = -9$).

3.3. Comparison with Bastian et al. (2012) and Chandar et al. (2014) Cluster Catalogs

Recently, studies by Bastian et al. (2012) and Chandar et al. (2014) have compared cluster catalogs in the galaxy M83, and have discussed how the selection of clusters can affect the resulting conclusions. In this section, we revisit this issue by comparing the HLA-generated catalogs used in the present study with the catalogs from these two studies in M83.

As described in more detail by Chandar et al. (2014), a comparison between three catalogs (Chandar-automatic, Chandar-manual, Bastian-hybrid) shows that about 70% of the clusters are in common when comparing any two of the three catalog. The biggest area of disagreement is for clusters with ages less than 10 Myr, with Bastian et al. including only relatively symmetric clusters while Chandar et al. also include slightly more diffuse, asymmetric clusters. The top panel in Figure 2 shows a color image of a region in M83 (see Chandar et al. 2014 to see the location of this region within M83). We invite the reader to make their own estimates of the likely clusters based on this figure before comparing with the cluster catalogs below. The reader might also want to go to the HLA (<http://hla.stsci.edu>) (image = HST_9774_of_ACS_WFC_F814W_F555W_F435W) to make the comparison using the interactive display, since the combination of a color image, contrast control, and ability to zoom can be very helpful.

The middle panel in Figure 2 shows a comparison of the HLA-generated cluster catalog used in the present study (large red circles) with the other three catalogs (Chandar-automatic in blue, Chandar-manual in yellow, Bastian-hybrid in purple—see Chandar et al. 2014 for a detailed description). The primary difference between the HLA-generated catalog and the other more “specialized” catalogs is that it does not go as deep. This is because the number of contaminants grows rapidly for magnitudes fainter than $M_I = -8$, which is therefore used as the cutoff for the HLA-generated catalog for M83. The more specialized catalogs can go deeper since either a manual step is included which guards against most contaminants, or in the case of the Chandar-automatic catalog, the parameters can be better tuned for a particular dataset.

The bottom panel of Figure 2 shows the results when comparable magnitude thresholds are used. The agreement is relatively good, with an average of 71% of the clusters in common, based on an average of all 12 pairwise comparisons between the four catalogs. More specifically, the average value is $75 \pm 8\%$ when the HLA-generated catalog is included in the comparison and $68 \pm 5\%$ when it is not (i.e., they are the same within the errors). Similar results are found for two other fields (one in a denser and one in a sparser region). These numbers are similar to those found in the comparisons reported in Bastian et al. (2012)

and Chandar et al. (2014). We conclude that the HLA-generated catalogs are of comparable quality, down to a threshold of $M_I = -8$.

A few comments on specific objects provides more insight into the relative strengths and weaknesses of each catalog. The automatic catalogs have more examples of close pairs of stars that are incorrectly selected as clusters (e.g., the red circle just above object 5652 and the upper right most blue circle). This is the primary type of contaminant included in the automatic catalogs at fainter magnitude, as discussed above. Another important difference is that the Bastian catalog has fewer objects in crowded regions with high backgrounds (e.g., 5652 and 5715 are not included in the Bastian catalog). This is the main reason for a discrepancy between the Chandar and Bastian catalog for clusters with ages < 10 Myr (i.e., since young clusters tend to be found in crowded regions), as discussed in both papers.

3.4. Differentiating Young and Old Clusters

Because there is color information for each of our target galaxies, we can make a general assessment about the ages of star clusters that dominate each galaxy sample, at least at the bright end where we have examined each cluster manually. This is important because the luminosity functions of ancient globular clusters are quite different from those of compact young star clusters. In particular, luminosity functions of young clusters tend to be well approximated by a power-law, while the luminosity (and mass) functions of old GCs have a pronounced deficit of objects below $M_I \approx -8.5$ ($\approx 2 \times 10^5 M_\odot$) and appear peaked when plotted in logarithmic bins.

Table 2 contains the total number of clusters brighter than $M_I = -9$ for each sample, as well as the I band magnitude of the brightest cluster. Table 2 also includes an estimate of the number of the brightest 10 clusters that appear to be red, ancient globular clusters, rather than young, blue clusters. We make this manual assessment based on the HLA color image. Ancient globular clusters can generally be distinguished by the fact that they; 1) have redder colors because they contain only low mass stars, 2) they have small variations in their pixel-to-pixel flux compared with younger clusters (e.g., Whitmore et al. 2011), 3) they tend to have larger half-light radii than many of the very young clusters (e.g., Bastian et al. 2012), and 4) they are generally found in uncrowded regions away from regions of recent star formation. One potential complicating factor is that a young cluster behind a dust lane can appear to have colors similar to an ancient globular clusters. However, these can generally be identified by a manual examination (i.e., no obvious dust lanes in the immediate area around the cluster). We will present a separate analysis of the old globular cluster systems in these galaxies in a future paper (Bowers et al. 2014). In Section 5.1 we find no statistically

significant differences in the luminosity functions for galaxies with significant “pollution” by old globular clusters.

3.5. Star Formation Rates

One of the goals of this study is to examine the $M_{\text{brightest}}$ vs. $\log N$ relation, and the related $M_{\text{brightest}}$ vs. $\log \text{SFR}$ relation. In this section we describe how we measure the SFR for our galaxies.

We derived star formation rates for each field using GALEX far-ultraviolet images and the calibration of SFR vs. UV continuum flux in Kennicutt (1998). The calibration assumes a constant star formation rate over time scales of $\sim 10^8$ years, as is probably appropriate for most of our targets, and is normalised to a Salpeter IMF with a minimum mass of $0.1 M_{\odot}$. The SFR and FUV continuum luminosity (here expressed as L_{λ}) are related as

$$\text{SFR} [M_{\odot} \text{yr}^{-1}] = 1.07 \times 10^{-40} L_{\lambda} [\text{erg s}^{-1} \text{\AA}^{-1}] \quad (1)$$

We obtained the FUV flux densities from the GALEV FUV (1500 \AA) images via the relation given on the GALEX web page¹ (see also Morrissey et al. 2007):

$$F_{\lambda} [\text{erg s}^{-1} \text{cm}^{-2} \text{\AA}^{-1}] = 1.40 \times 10^{-15} \text{CPS} \quad (2)$$

where CPS are the counts-per-second measured in the GALEX frames. The flux densities were converted to luminosities using the distances and foreground extinctions in Table 1. The FUV extinction was computed assuming the relation between $E(B - V)$ and A_{FUV} in Hunter et al. (2010), $A_{\text{FUV}} = 8.24 E(B - V)$.

We note that the star formation rates were computed for the sections of the galaxies covered by the ACS/WFC footprints rather than for the whole galaxies. In practice, this was done by transforming the ACS images to the GALEX frames with the SREGISTER task in the IMAGES.IMMATCH package in IRAF and then masking out the regions of the GALEX frames that were not covered by the ACS images. These star formation rates are compiled in Table 1.

¹http://galexgi.gsfc.nasa.gov/docs/galex/FAQ/counts_background.html

4. Star Cluster Luminosity Functions

In this section, we present luminosity functions for star clusters in our program galaxies. Previous works have found that luminosity functions of star clusters can be described, at least approximately, by a power law, $\phi(L) \propto L^\alpha$. We first discuss three different techniques we use to determine α in Section 4.1. Results using different selection criteria for a single galaxy (M83) are discussed in Section 4.2, followed by a discussion of the entire galaxy sample in Section 4.3. A comparison between our predicted uncertainties, and empirical estimates of uncertainties (e.g., by comparing different parts of the same galaxy) is made in Section 4.4.

4.1. Techniques for Determining α

Three different methods are used in this paper for the determinations of α . The first two methods are simple fits to a binned luminosity function, one with constant sized magnitude bins— $\alpha_{\text{const-mag}}$ and the other with fixed number of clusters per bin $\alpha_{\text{const-number}}$. See Maiz-Apellaniz & Ubeda (2005) for a discussion of the pros and cons of the two methods.

The third method uses a maximum likelihood power-law to fit the luminosity function. This method is independent of any binning of the data. If the LF is assumed to be a power-law $dN/dL \propto L^\alpha$ for $L_{\min} \leq L \leq L_{\max}$, the likelihood $\mathcal{L}(L|\alpha)$ of observing a dataset $L = \{L_1, L_2, \dots, L_n\}$ for a given α is given by

$$\mathcal{L}(L|\alpha) = \left(\frac{\alpha + 1}{L_{\max}^{\alpha+1} - L_{\min}^{\alpha+1}} \right)^n \prod_{i=1}^n L_i^\alpha \quad (3)$$

Numerically, it is more convenient to work with the logarithmic likelihood,

$$\log \mathcal{L}(L|\alpha) = n \log \left(\frac{\alpha + 1}{L_{\max}^{\alpha+1} - L_{\min}^{\alpha+1}} \right) + \alpha \sum_{i=1}^n \log L_i \quad (4)$$

The maximum likelihood estimate of the slope, α_{best} is then the value for which $\log \mathcal{L}(L|\alpha)$ is maximized. Once α_{best} has been found, we estimate the 1- σ confidence interval $\alpha_{\text{best}} \pm \sigma_\alpha$ as

$$\frac{\int_{\alpha_{\text{best}} - \sigma_\alpha}^{\alpha_{\text{best}} + \sigma_\alpha} \mathcal{L}(L|\alpha) d\alpha}{\int_{-\infty}^{\infty} \mathcal{L}(L|\alpha) d\alpha} = 0.68 \quad (5)$$

The value of α determined using this method will be denoted $\alpha_{\text{max-likelihood}}$.

4.2. The Effect of Changing Values of C and R_{neighbor} on the Determination of α Using M83 as a Test Case

In this section we assess the impact that our selection criteria have on the resulting cluster luminosity functions. In order to accomplish this, we use the HLA catalog of field 1 of M83 (NGC 5236), and vary the values of concentration index C and R_{neighbor} (used by the UNIQPOS algorithm) discussed in Section 3.2. For M83 we found that the combination of $C \geq 1.15$ and $R_{\text{neighbor}} = 20$ pixels gives the best results in terms of separating the stars from clusters with the fewest number of contaminants down to a limiting magnitude of $M_I = -8$. In Figure 3, we present nine different combinations, with C values greater than 1.10, 1.15, and 1.20, and $R_{\text{neighbor}} = 10, 20, 30$ pixels. These parameters span the range that produces reasonable cluster catalogs in M83; going beyond these ranges results in catalogs that are clearly non-optimal based on manual examinations.

The resulting values of α range from -2.22 (for $C = 1.20$, $R_{\text{neighbor}} = 30$) to -2.37 (for $C = 1.15$, $R_{\text{neighbor}} = 10$). The mean for all nine determinations is -2.30 ± 0.05 . This compares well with our preferred value of -2.32 ± 0.08 based on the fit with $C \geq 1.15$ and $R_{\text{neighbor}} = 20$ (i.e., the central panel).

A similar exercise has been performed using magnitude thresholds with values $M_I = -7, -7.5, -8.0, -8.5, -9.0$ magnitude (all with values of $C \geq 1.15$ and $R_{\text{neighbor}} = 20$) in M83. We find the values of α range from -2.38 at -7.5 to -2.28 at -8.5 , with a mean value of -2.34 ± 0.04 , again in good agreement with our preferred value. We also note that the fraction of contaminants (primarily pairs of stars—see Section 3.2) ranges from about 50% at $M_I < -7$ mag to 20% at $M_I < -8$ mag (similar to the results obtained in Section 5.2 for NGC 1300 and NGC 5457) to about 10% at $M_I < -9$ magnitude, based on visual examination.

We conclude from these exercises that the adopted parameters for our best M83 cluster catalog (i.e., magnitude threshold $M_I < -8$ magnitude, $C \geq 1.15$ and $R_{\text{neighbor}} = 20$) are near optimal, given our particular algorithms for selecting the clusters. Reasonable values of C and R_{neighbor} result in changes to α at about the 0.1 level. Care needs to be taken when determining the magnitude limit to guard against the inclusion of large fractions of contaminants when producing automatic catalogs.

4.3. Cluster Luminosity Functions for the Entire Galaxy Sample

Next, we examine the results for the “best” cluster catalogs for all the galaxies in the sample. These catalogs were constructed using the C and R_{neighbor} values reported in Table 2,

down to the magnitude limit given in column 2 of the table. We compile the best fit values of α for each of these catalogs in Table 3, for the max-likelihood and const-number fits. The const-magnitude fits give similar results.

Figure 4 shows a comparison of the values of $\alpha_{\text{max-likelihood}}$ with $\alpha_{\text{const-number}}$. While the mean values are in reasonably good agreement (i.e., $\Delta = -0.08 \pm 0.14$, and the agreement is good in the range $\alpha = -1.8$ to -2.5 , there is a tendency for the $\alpha_{\text{max-likelihood}}$ values to be more negative than the $\alpha_{\text{const-number}}$ values for the steeper LFs.

Overall, based on Figure 5, the cluster luminosity functions in all of our sample galaxies appear to be reasonably well described by a single power-law. There is no obvious evidence for a break or change in slope at either the bright or faint end of these distributions (at least based on Figure 5), a topic that we will revisit in Sections 5.1 and 5.2.

Figure 5 shows the luminosity functions for each of our 20 program galaxies. We find values of the power-law indices, $\alpha_{\text{const-number}}$, that range from approximately -1.95 (NGC 4395) to -2.80 (NGC 1483—however, note that the estimated error for this galaxy is 0.65). This is a somewhat broader range, reaching slightly steeper values, than found in most studies to date. For example, Larsen (2002) finds a range from -2 to -2.4 for 6 spiral galaxies. He also found a weak tendency for steeper slopes among fits to the brighter magnitudes. This might be part of the reason for steeper slopes in our results, since the limiting magnitude for our study was roughly a magnitude brighter than in the Larsen (2002) study.

4.4. Empirical Determination of Uncertainties

The mean estimated uncertainties as returned by the software for the various methods of determining values of α in Table 3 are 0.19 (maximum likelihood) and 0.21 (constant number). The empirical scatter between determinations for each galaxy using the two methods is 0.14 magnitude, providing evidence that the estimated uncertainties are fairly accurate, and may actually be slightly overestimated.

We can make additional empirical determinations of the true uncertainties by comparing fields which have been observed in two different fields for three of the galaxies (i.e., NGC 1300, NGC 5236, and NGC 5457). There is no guarantee that the different fields have the same values of α , hence this should be considered an upper limit. However, we note that in all three cases, the two fields are roughly the same radii from the center of the galaxy (see Figure 1), hence any trends caused by radial gradients would be minimized. The mean differences are 0.33 (maximum likelihood) and 0.19 (constant number), in reasonable agreement with the numbers quoted in the first paragraph.

We conclude that a typical value for the uncertainty in the determination of α for our galaxies is in the range 0.15 to 0.20. The overall scatter in the values of α for the entire sample of galaxies are 0.27 for maximum likelihood and 0.18 for constant number fits, comparable, or slightly larger than our predicted uncertainties. This suggests that much of the observed spread in values of α for the entire sample is due to statistical noise, rather than real differences between the galaxies.

Perhaps a better test of the degree to which the observed scatter is real can be made by only including galaxies with error estimates < 0.2 . In this case we find mean values of -2.39 (maximum likelihood) and -2.35 (constant number) with values for the observed scatter of 0.21 and 0.14. The mean for the two methods yields -2.37 and a scatter of 0.18. We adopt these as our best-guess values for the remainder of the paper.

The mean of the estimated uncertainties returned by the software, as listed in Table 3, are 0.13 and 0.11 for this subset of high S/N galaxies. If accurate, this suggests that roughly 1/2 of the observed scatter is real (i.e., by subtracting the observed and estimated errors in quadrature). The weak correlations discussed in Section 5.1 and 5.2 provide further evidence that at least some of the observed scatter is real.

Table 3 includes a compilation of α estimates from other studies. The mean difference between our constant number bin measurements of α and others is 0.12 with a scatter of 0.16. This again supports our conclusion that the mean uncertainty in our estimates of α is about 0.15 magnitude (for the higher S/N galaxies), and also demonstrates the result that we tend to find somewhat steeper values of α than many past studies.

5. Results and Discussion

5.1. Searching for Correlations with the Slope of the Luminosity Function

Figure 6 shows a plot of α vs. the following parameters: a) log SFR, b) distance modulus (DM), c) $M_{\text{brightest}}$, d) log N, e) Hubble type (T), and f) absolute B magnitude (M_B). The α values used in Figure 6 are from the constant number fits. The maximum likelihood fits show similar correlations but with slightly more scatter, similar to the results discussed in Section 4.

The significance of each correlation (in units of σ , defined as the slope of the correlation divided by the uncertainty in the slope of the correlation) is provided in each panel. Typical differences between the two methods are about 0.5σ .

The open circles in Figure 6 show the galaxies with very few clusters (i.e., $\log N < 1.2$

for the $M_I = -9$ limit: see Table 2) while the solid circles (i.e., the high S/N sample) show the 16 galaxies with $\log N > 1.2$. The significance of the correlations using both the full and high S/N samples are included in Figure 6.

The strongest correlation (2.8σ) for the full sample is with Hubble Type (T); with later-type galaxies having less negative values of α (i.e., a flatter LF). It appears that the correlation may actually be slightly U-shaped, with the earlier types $T < 4$ (i.e., Sbc and earlier galaxies) also showing slightly lower values of α . If we restrict the range to $T > 4$ (i.e., later than Sbc galaxies) the correlations becomes even better (i.e., 4σ —see Figure 6). We note, however, that removing NGC 4038/39 (the Antennae) reduces the correlations by about a factor of 2.

The next best set of correlations for the sample are with $M_{\text{brightest}}$, $\log N$, and $\log \text{SFR}$, with a value of 2.0σ being reached for the constant number fits for $M_{\text{brightest}}$. The $M_{\text{brightest}}$ correlation for the high S/N galaxies reaches a value of 4σ . In all cases the trend is in the sense of the galaxies with more star formation (hence more clusters and a brighter values of $M_{\text{brightest}}$ due to the size-of-sample effect) having lower values of α . It is already well known that these three parameters correlate with each other well, as shown in Figure 7. This will be discussed in more detail in Section 5.3. Hence, these three correlations are probably manifestations of the same underlying correlation. We note, however, that removing NGC 4038/39 (the Antennae) reduces the correlations by about a factor of 2 in these 3 cases.

We also note that the use of larger apertures (radii = 7 pixels) in an attempt to minimize the dependence on mean aperture corrections, as discussed in Section 3.2, has only a minor effect on the results shown in Figure 7. The slopes in the bottom two plots change by only 1 or 2 percent (in both cases becoming slightly flatter) when using the larger aperture measurements. The scatter and the statistical significance improve, with values of $\text{RMS} = 0.44 \text{ mag}$ and 10.6σ for the $M_{\text{brightest}}$ vs. $\log N$ relation and $\text{RMS} = 0.36 \text{ mag}$ and 12.4σ for the $M_{\text{brightest}}$ vs. $\log \text{SFR}$ relation. The scatter in these diagrams is remarkably low!

The inclusion of low S/N data points may mask real correlations. When only the high S/N galaxies (solid points) are included in the fit we find that the correlations improve in some cases (e.g., with $M_{\text{brightest}}$ and $\log N$), but get worse in others (e.g., Hubble Type).

There may also be a weak correlation with the absolute B magnitude of the galaxy (M_B), though this becomes weaker for the higher S/N sample.

We note that there is little or no correlation with the distance modulus (DM). This is reassuring and demonstrates that strong biases are not introduced by differences in spatial resolution. Finally, there is no significant correlation between α and the fraction of red (old) clusters, as discussed in 3.4 (not shown).

Figure 8 shows the correlations between Alpha (α) and Hubble type (T) using six different methods. This provides an indication of how robust our results are. The first three examples show the effect that different methods of fitting the luminosity functions have on the results (i.e., the maximum likelihood, constant number and constant magnitude methods defined in Section 4.1). The other panels show the effects of using larger apertures, and the brighter part of the LF. The high S/N dataset is used for all six panels along with a requirement that there be at least twenty clusters in the sample for each individual galaxy. In all cases a weak 1.3 to 2.5σ correlation is found. The constant bins fitting method gives the smallest scatter and has therefore been used as our primary method for most of this paper.

The bottom row of Figure 8 shows the results when using 7-pixel photometry (using the constant magnitude method), as discussed in Section 3.2, in an attempt to minimize the dependence on aperture corrections. The same general trend is seen although with larger scatter. The two panels labeled “bright” show similar estimates but with a faint magnitude limit which is 1 magnitude brighter, in an attempt to determine whether there is a turn-down at the bright end of the luminosity function. In both cases there is a marginal 0.1 magnitude trend for the brighter fits to be steeper, suggesting a possible turn-down. However, this represents less than a 1σ difference in both cases. This point will be revisited in Section 5.2.

We finish by noting that while there do appear to be some weak correlations present, perhaps the main result is the apparent similarity of the values of α over a relatively wide range of galaxies. This suggests that to first order, the LFs are fairly universal, similar to results for mass functions (e.g., Whitmore et al. 2007 and Fall and Chandar 2012—but see also Bastian et al. 2012 and Chandar et al. 2014). However, with the availability of a relatively large sample of galaxies (20), and using a more uniform set of data and analysis techniques than has been possible in the past, it appears that we are beginning to detect weak second-order effects that may be important for understanding the physics behind the demographics of cluster formation and destruction.

5.2. The Luminosity Function of “Super Galaxies”

The cluster lists produced in this work can be combined in different ways to improve statistics and to explore more subtle features in the shape of the luminosity functions. Here, we create cumulative distribution functions (CDFs) for “super galaxies” by combining galaxies as a function of: 1) total brightness in the B band (i.e., M_B), 2) \log SFR, and 3) Hubble Type. Three subdivisions are included in each case (see notes to Table 3 for details). The Antennae galaxy, NGC 4038/39 has been left out of this exercise since it is a merger remnant

and hence may have different properties than normal spiral galaxies (i.e., it has one of the flattest LFs). In support of this possibility, Randriamanakoto et al. (2013) report flatter LF’s for their sample of LIRG galaxies, most of which are mergers.

The data used to define these CDFs have been fit in the same way as the single galaxy luminosity functions; the results are compiled in Table 3. Figure 9 shows the CDFs for various composite galaxies. Dashed lines show power law slopes of -2.0 (flattest), -2.5 , and -3.0 (steepest) for reference.

We first note that most of the fits for α are between -2.0 and -3.0 limits, with values around -2.5 being most typical. This is consistent with values for α in Table 3 and Figure 6, as expected. We find that a few of the CDFs tend to steepen at the bright end, providing tentative evidence of a turn-down. However, it should be kept in mind that this represents a very small number of clusters (i.e., generally the brightest 5–10 clusters out of several thousand, i.e., less than 1% of the data).

The graphical overemphasis on a relatively small number of bright clusters, which is implicit when showing cumulative distribution functions on a log scale, complicates comparisons with the regular power law fits of α listed in Table 3. For example, based on the full CDF for the $0.3 M_{\odot} \text{ yr}^{-1}$ sample (i.e., the green line in the small inset of the middle panel of Figure 9) one might conclude that $\alpha \approx -3.0$. However, Table 3 gives a value of -2.54 . This is because the vast majority of the clusters are faint (e.g., 77% are fainter than $M_I = -10$), and the slope is flatter in this magnitude range, as shown by a close look at the middle panel in Figure 9. The 50% and 1% points are included in Figure 9 to reinforce this point.

Of the nine composite galaxies shown in Figure 9, eight appear to have a downturn (i.e, the slope changes by more than 0.25 relative to the fiducial -2 , -2.5 , -3 slopes as one goes from the 50% point to the 1% point). The remaining case (Sc–Scd galaxies) has a relatively straight CDF in this range; no CDF has an upturn at the bright end. If we do a similar analysis of the individual galaxies (not shown), where low-number statistics are often an issue, we find that eight of the galaxies appear to have a downturn in their LFs, six appear relatively constant, and only two appear to have upturns. Hence, there does appear to be some evidence for a downturn at the bright end of most of the CDFs. This is similar to the results discussed in Section 5.1 for the LFs.

A potential concern about the reality of the apparent downturn at bright magnitudes is the fact that we manually inspected the top 10 clusters in each galaxy and removed contaminants (e.g., foreground stars, galactic nuclei, background galaxies—see Section 3.2). This could, in principle, cause part of the downturn since we have not done the same for the fainter cluster candidates.

We can estimate the effect this might have by spot-checking a few of the galaxies at the fainter magnitudes to determine the fraction of contaminants. Based on manual inspections of NGC 1300 and NGC 5457, we find the following fractions of contaminants. For M_I in the range -10.5 to -10 magnitude we find $12 \pm 6\%$, for M_I from -10.0 to -9.5 magnitude we find $5 \pm 2\%$, and for M_I in the range -9.5 to -9 magnitude we find $5 \pm 2\%$ contaminants. We conclude that the contaminant fractions are typically quite small, and are relatively constant as a function of M_I . Even if there were $\approx 20\%$ differences as a function of magnitude from brightest to faintest, this would only introduce changes in α which are comparable to our statistical uncertainties (i.e., ≈ 0.1).

We conclude that there is evidence that many of the galaxies have a small downturn in their CDFs at bright magnitudes. While the LF is clearly related to the MF, there is not a simple 1:1 correspondence between the two (e.g., see Fall 2006 and Larsen 2009). Hence, we are not able to make a similar statement about the MF. We leave a detailed investigation of this issue for the future.

We now look at each of the three categories of composite galaxies in turn, starting with the M_B compilations on the top. We find a possible weak trend for the CDF to be steeper for lower luminosity galaxies at the 50% point. However, the trend is essentially gone by $M_I = -11$. In addition, the trends in Figure 6 are not very significant, and are actually in the opposite direction. Hence we conclude that there is no clear correlation for α to change as a function of M_B .

We next turn to the 3 SFR categories as shown in the middle panel of Figure 9. We find an apparent trend, with a steep slope for the low SFR galaxies (-2.88 ± 0.22), and shallower slopes for the intermediate SFR category (-2.56 ± 0.09) and for the high SFR category (-2.54 ± 0.08). As discussed in the previous section, the same weak trend (and the associated $M_{\text{brightest}}$ vs. $\log N$ relationship) can be seen in Figures 6, providing additional evidence that this correlation is real.

The bottom panel shows the Hubble type composite galaxies. We have already seen in Figures 6 and 8 what appears to be a weak correlation between values of α and T. In Figure 9, we see some evidence for the early type galaxies to be shallower, at least down to about $M_I = -10.5$ mag. However, there is no clear trend for the Sd–Sm galaxies to be different than the Sc–Scd galaxies. The values for α for the three Hubble type categories listed in Table 3 also give ambiguous results. Hence, the weak tendencies suggested by Figures 6 and 8 should be considered tentative. In particular, we note that the removal of the Antennae would reduce the apparent correlation in Figure 6 by about a factor of two.

For this reason, the Antennae has been left out of the supergalaxy compilations and is

shown separately in Figure 9. As expected, the CDF for the Antennae is significantly flatter than cumulative distributions for the other galaxies (note that due to incompleteness fainter than $M_I = -10$ mag, we have extrapolated down to $M_I = -9$ mag, as shown by the dotted line). This flatter slope is supported by Table 3 where the Antennae has the 2nd flattest slope of all 20 of the program galaxies. Only NGC 4395, with large uncertainties due to very few clusters, has a flatter slope.

5.3. $M_{\text{brightest}}$ vs. log N and $M_{\text{brightest}}$ vs. log SFR Relationships

One of the goals of our study is to examine whether star formation in violent environments is fundamentally different than star formation in quiescent settings. Whitmore (2003) addressed this question by making a plot of the brightest cluster ($M_{\text{brightest}}$) versus the log of the number of clusters brighter than $M_I = -9$ mag (log N) in a galaxy. If there are two modes of star formation we might expect this distribution to be bimodal. However, the distribution is continuous, with a well defined correlation that can be explained by simple statistics; e.g., by drawing different size samples from the same $dN/dL \propto L^{-2}$ luminosity function. This is often referred to as the “size-of-sample” effect. Hence, it appears that the processes involved in the formation of star clusters are largely universal, and do not depend strongly on the environment.

Larsen (2002) confirmed this result in the form of the $M_{\text{brightest}}$ vs. log SFR relationship, and more recently, several authors have added additional data or developed more sophisticated analysis techniques (Whitmore, Chandar & Fall 2007; Bastian et al. 2008; Larsen 2009; Vavilkin 2011) .

Unfortunately, the data points used in these studies have several observational shortcomings. For example, they often use a very inhomogeneous data set (e.g., a mixture of ground-based and space-based observations, different wavelength ranges requiring extrapolations to the V band, different analysis techniques since they originate from different papers, etc.). Using the results of the present, more homogeneous sample, we are now in a better position to re-examine this question.

The top panel of Figure 10 shows the results for the 20 galaxies in our sample (note that there are actually 23 points since we have 3 galaxies with two separate fields of view). Two galaxies have completeness issues (i.e., NGC 6217 and NGC 4038/39 are only complete to $M_I = -10$ mag). A correction has been made to these galaxies by measuring the fractional increase in the number of clusters brighter than -10 mag to the number brighter than -9 mag for NGC 1309, NGC 2397, and NGC 3627, and then applying this correction to the

two incomplete galaxies. The resulting correlation in Figure 10 is quite tight with a slope -1.97 ± 0.22 , RMS scatter = 0.53 mag and 8.9σ level of significance. We note that this value is consistent with a value of -1.82 that would be predicted purely by statistics by a $L_{\text{brightest}} \propto N^{-1/(1+\alpha)}$ dependence with a value of $\alpha = -2.37$ for the LFs in the sample (see Larsen 2009).

Hence, our uniform database does appear to result in smaller scatter in the $M_{\text{brightest}}$ vs. log N relationship than has been seen in past studies (e.g., Larsen 2002 finds RMS scatter = 0.9 magnitude).

The bottom panel of Figure 10 shows the related $M_{\text{brightest}}$ vs. log SFR diagram. Two additional datasets for LIRGs have been added to the diagram: 1) Bastian et al. 2008 (triangles) and 2) Vavilkin 2011 (asterisks). We note that part of the reason for the large difference between the SFR of our predominantly nearby spiral sample and the more distant LIRG sample is that the field-of-view for our sample of spiral galaxies typically includes only a portion of the galaxy, while the entire galaxies are included in the more distant LIRG samples. Nevertheless, most of the difference in SFR is real, with the LIRG galaxies often having SFRs that are orders of magnitude larger than spiral galaxies.

An advantage of the log SFR version of the relationship is that it also allows us to include dwarf galaxies, which may not have a $M_I = -9$ mag cluster needed to define log N. Figure 10 shows that the correlation extends over roughly six orders of magnitude, from dwarf galaxies to ULIRGS. The slope for the $M_{\text{brightest}}$ vs. log SFR relationship is -1.73 ± 0.08 , similar to both the $M_{\text{brightest}}$ vs. log N value (-1.97 ± 0.22) and the prediction from Larsen 2009 (-1.82) discussed above.

The scatter for the LIRG samples is 0.90 magnitude (with IC5283 and Arp 220 removed), considerably larger than for our spiral sample (i.e., 0.41 magnitude in Figure 7). This is partly due to the higher levels of extinction present in many of the LIRG galaxies, as shown by the corrections for IC5283 and Arp 220 (Vavilkin, 2011), which bring the galaxies back into line (see Figure 10). Another potential concern is the effect of spatial resolution for the more distant galaxies. Are some of the more luminous “clusters” in distant galaxies really several clusters blended together? Randriamanakoto et al. (2013) have performed simulations based on degraded images of the Antennae galaxies which indicates that this is not likely to be a serious problem for the modest redshifts of most of our target galaxies.

6. CONCLUSIONS

Hubble observations using the ACS/WFC camera have been used to construct star cluster luminosity functions for 20 nearby, star-forming galaxies. Automatically generated source lists from the Hubble Legacy Archive (HLA) were employed for the project. These catalogs provide the largest set of uniform, automatically-generated cluster candidates we are aware of in the literature at present. The primary results are listed below.

1. Comparisons with other recently generated cluster catalogs (e.g., Bastian et al. 2012; Chandar et al. 2014) demonstrate that the HLA-generated catalogs are of similar quality, but in general do not go as deep as manually-generated catalogs.

2. A single power-law of the form $dN/dL \propto L^\alpha$ has been used to approximate the LF using three different fitting techniques: constant number and constant magnitude binning (e.g., see Maiz-Appellaniz & Ubeda 2005 and Chandar et al. 2010 for discussions), and a maximum likelihood method that does not require binning. The methods give comparable results, although there may be a tendency for the maximum likelihood method to give more negative values of α for the steeper LFs.

3. Using the mean from the two methods and the high S/N sample, the average value for α is -2.37 , with a RMS scatter = 0.18 when using the F814W (“ I ”) band. Our values of α are generally steeper than most past studies, with a difference of $\delta = 0.12 \pm 0.16$ when comparing galaxies one-to-one.

4. A weak correlation is found for galaxies with high values of the SFR (or equivalently galaxies with the brightest clusters or the largest number of clusters) to have shallower values of α . The same trend is found for α from composite “supergalaxies” with different SFRs, strengthening the case for the reality of this correlation. In addition, the Antennae galaxy (NGC 4038/39), a merging system with a relatively high star formation rate, has the second flattest luminosity function in the sample.

5. A weak correlation may be present between α and Hubble Type in the sense that later type galaxies (Sd–Sm) have lower values of α . However, the cumulative distribution functions (CDFs) show mixed results, hence this result should be considered tentative.

6. While there appear to be some weak correlations, the relative similarity in the values of α for a large number of star-forming galaxies suggests that, to first order, the LFs are fairly universal. This is similar to results for mass functions (e.g., Whitmore et al. 2010 and Fall and Chandar 2012—but see also Bastian et al. 2012 and Chandar et al. 2014).

7. An exercise using larger aperture photometry (radii = 7 pixels) shows that the use of mean aperture corrections for small aperture photometry does not affect our results in a

substantial way.

8. Based on both the LFs and the cumulative distribution function (CDFs) of composite “super-galaxies,” we find some evidence for a downturn at the bright end of the luminosity functions, although it only pertains to about 1% of the clusters.

9. The $M_{\text{brightest}}$ vs. $\log N$ relation shows a small RMS scatter (0.4 to 0.5 mag). It appears that the reason that galaxies with more clusters have brighter clusters is primarily a statistical “size-of-sample” effect rather than being due to differences in the environments of starburst and quiescent galaxies. This is consistent with results found by Whitmore (2003) and Larsen (2002). The results for the $M_{\text{brightest}}$ vs. $\log \text{SFR}$ relationship are similar, with even a smaller scatter (≈ 0.4 mag).

10. The sample has been increased by including observations of both dwarf galaxies and LIRGS from studies by Bastian et al. (2008) and Vavilkin (2010). This shows that the $M_{\text{brightest}}$ vs. $\log \text{SFR}$ correlation extends over roughly six orders of magnitudes. However, higher levels of extinction appear to lead to larger scatter (0.9 magnitude) for the LIRG sample.

The photometric catalogs used in this study are available at:
<http://archive.stsci.edu/prepds/starclust-sfgal/>.

We thank the referee for several useful comments. BCW acknowledges the use of STScI grant GO-11781 and the summer student program at STScI for support of this project.

REFERENCES

- Bastian, N. 2008, MNRAS, 390, 759
- Bastian, N., Adamo, A., Gieles, M., Silva-Villa, E., Lamers, H. J. G. L. M., Larsen, S. S., Smith, L. J., Konstantopoulos, I. S., & Zackrisson, E. 2012, MNRAS, 419, 2606
- Bertin, E. 1996, A&AS, 117, 393
- Bowers, A. S., et al. 2014 in press
- Chandar, R., et al. 2014 in press
- Chandar, R., Fall, S. M., & Whitmore, B. C. 2010, ApJ, 711, 1263
- Dolphin, A. E., Kennicutt, R. C. 2002, AJ, 124, 158
- Fall, S. M. 2006, ApJ, 652, 1129
- Fall, S. M., & Chandar, R. 2012, ApJ, 752, 7

- Holtzman, J. A., Burrows, C. J., Casertano, S., Hester, J. J., Trauger, J. T., Watson, A. M., & Worthey, G. 1995, *PASP*, 107, 1065
- Hunter, D. A., Elmegreen, B. G., & Ludka, B. C. 2010, *AJ*, 139, 447
- Johnson, C. L., et al. 2012, *ApJ*, 752, 23
- Kennicutt, R. C., Jr. 1998, *ARA&A*, 36, 189
- Larsen, S. S. 2002, *AJ*, 124, 1393
- Larsen, S. S. 2009, *A&A*, 494, 539
- Maiz-Apellaniz, J., Ubeda, L. 2005, *ApJ*, 629, 873
- Miller, B. W., Whitmore, B. C., Schweizer, F., & Fall, S. 1999 *AJ*, 114, 2381
- Mora, M. D., Larsen, S. S., Kissler-Patig, M. 2009, *A&A*, 464, 495
- Mora, M. D., Larsen, S. S., Kissler-Patig, M., Brodie, J. P., & Richtler, T. 2009, *A&A*, 501, 949
- Morrissey, P., et al. 2007, *ApJS* 173, 682
- Portegies Zwart, S., McMillan, S., & Gieles, M. 2010, *ARA &A*, 48, 431
- Randriamanakoto, Z., et al. 2013, *MNRAS*, in press
- Sirianni, M., et al. 2005, *PASP*, 117, 1049
- Stetson, P. B. 1987, *PASP*, 99, 191
- Whitmore, B. C. 2003, The Formation of Star Clusters, in “A Decade of HST Science,” eds. Mario Livio, Keith Noll, & Massimo Stiavelli (Cambridge: Cambridge University Press), 153
- Whitmore, B. C., et al. 2011, *ApJ*, 729, 14
- Whitmore, B. C., Chandar, R. C., & Fall, S. M. 2007, *AJ*, 133, 1067
- Whitmore, B. C., Chandar, R., Schweizer, F., Rothberg, B., Leitherer, C., Rieke, M., Rieke, G., Blair, W. P., Mengel, S., & Alonso-Herrero, A. 2010, *AJ*, 140, 75
- Vavilkin, T. 2011, Thesis, State University of New York at Stony Brook

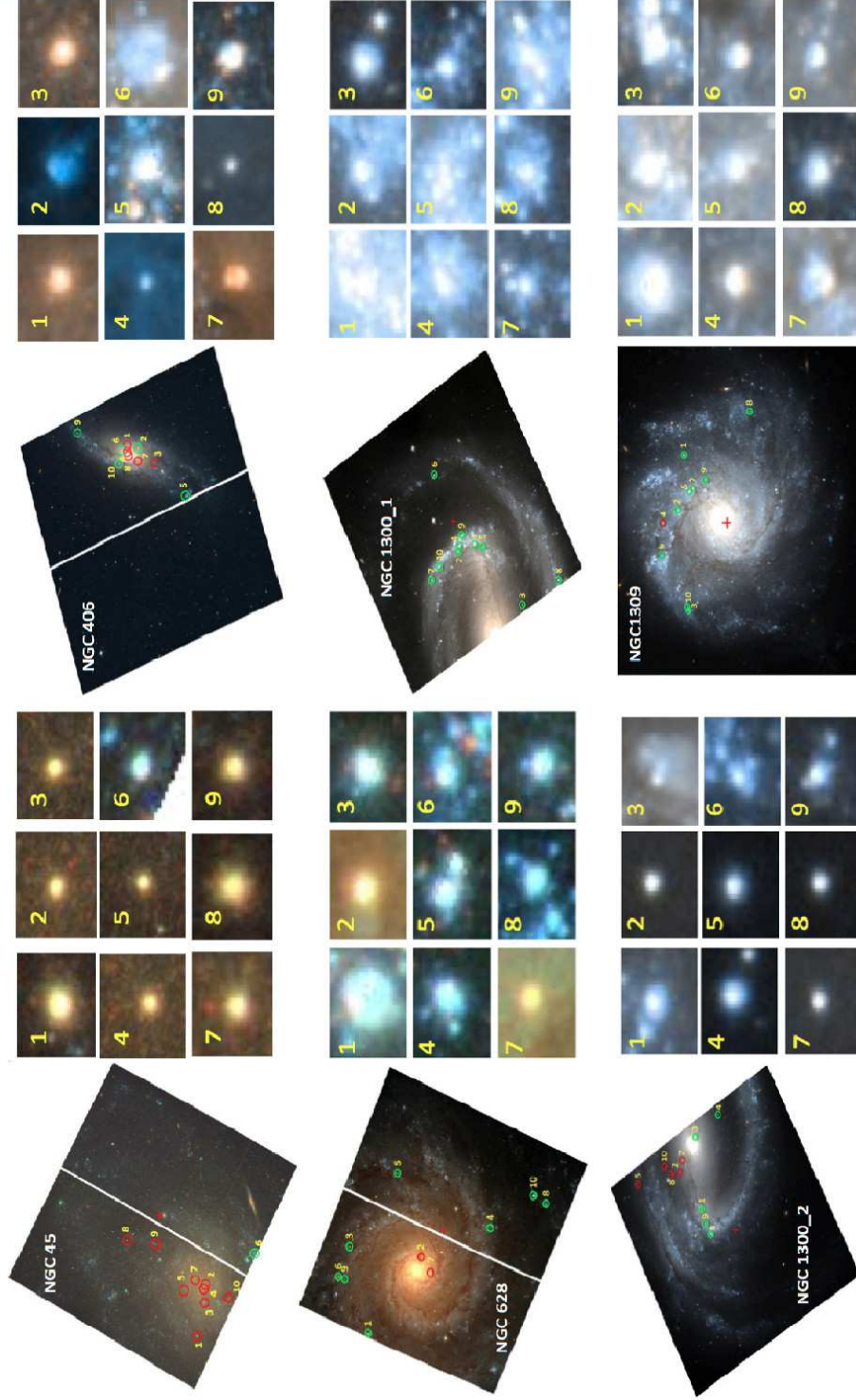


Fig. 1a.— Color images of the 20 galaxies used in this work. Red circles show young (blue) clusters while green circles show old clusters. $5 \times 5''$ cutouts of the 9 brightest sources in each HLA catalog are also shown.

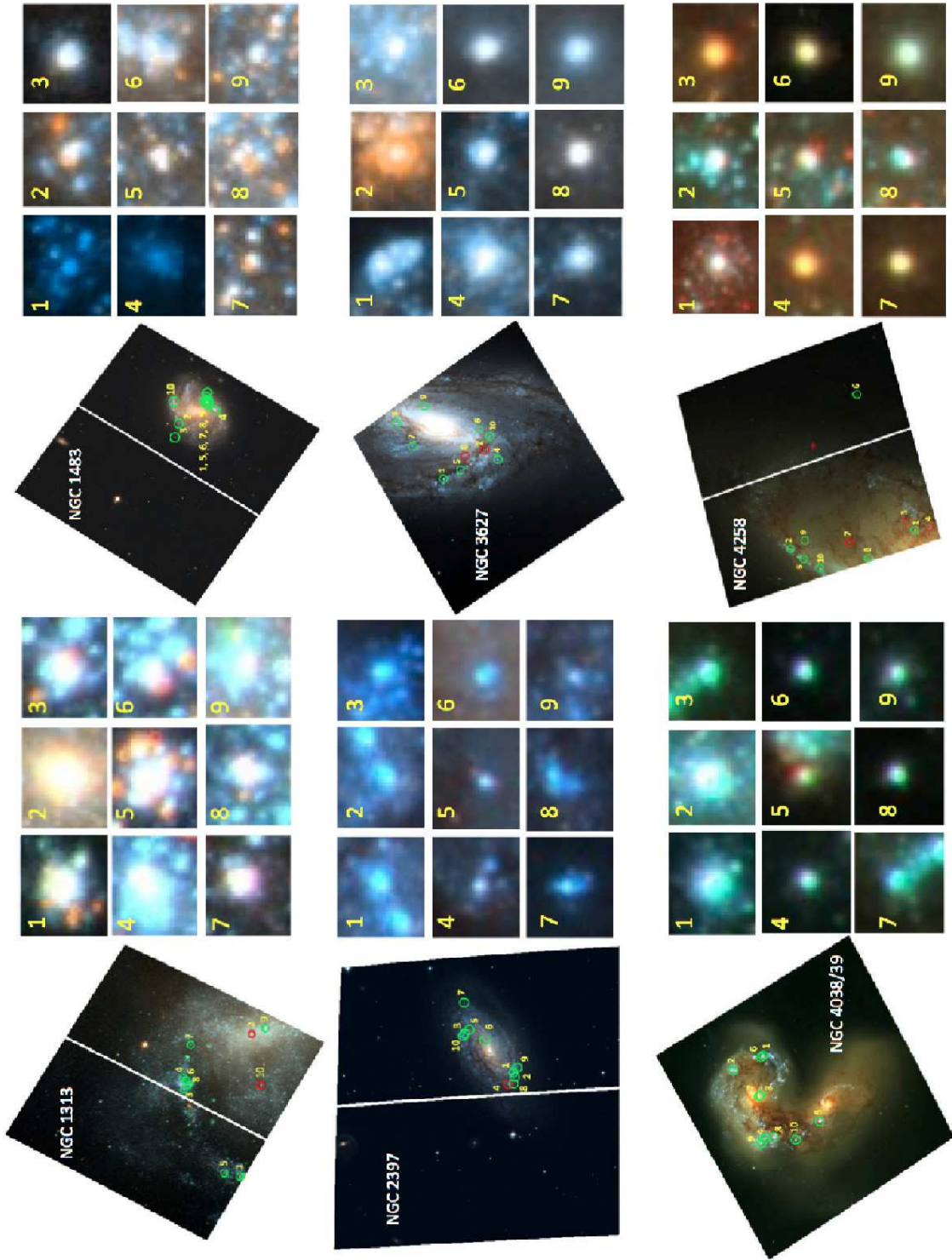


Fig. 1b.— Continued.

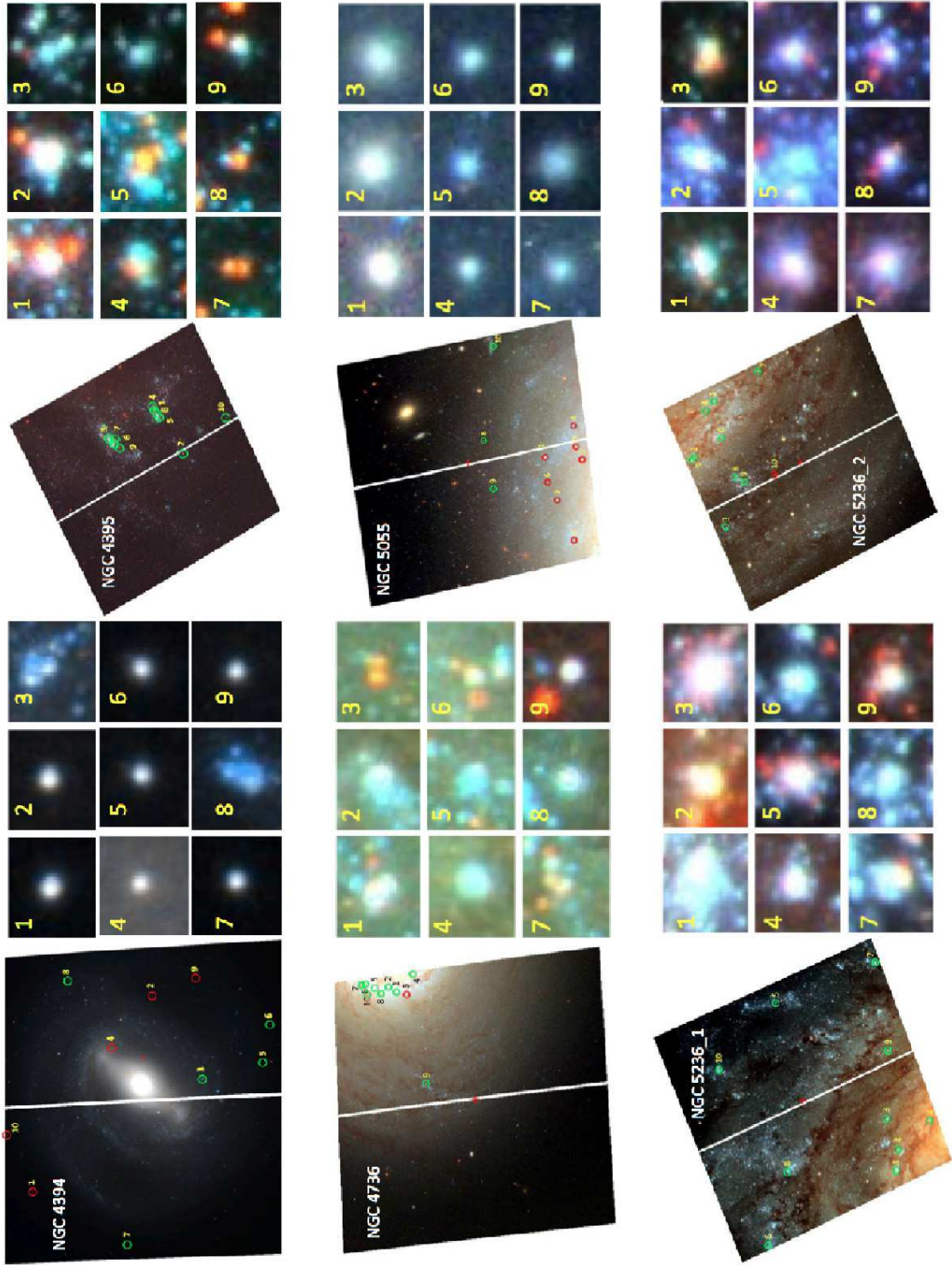


Fig. 1c.— Continued.

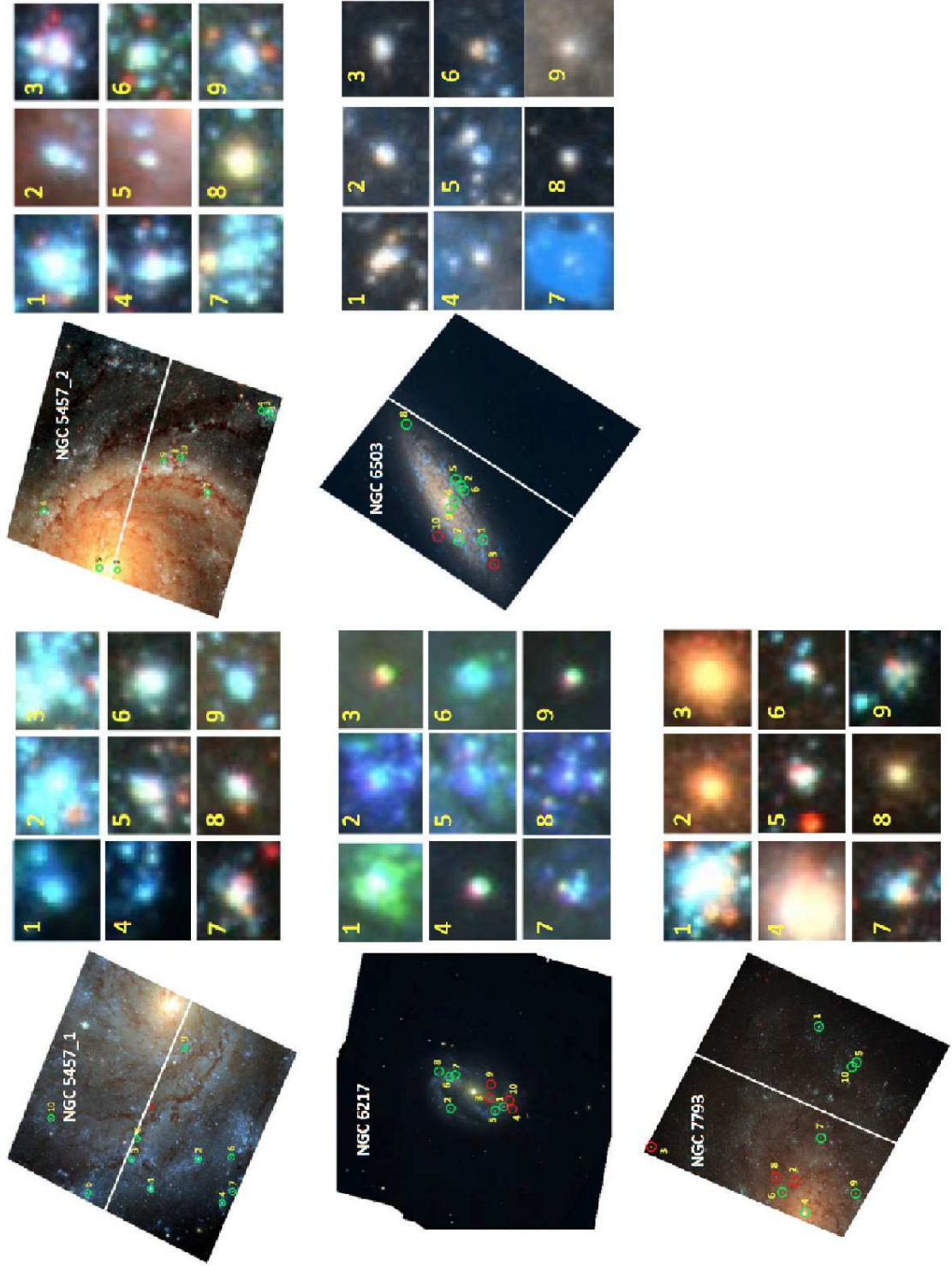


Fig. 1d.— Continued.

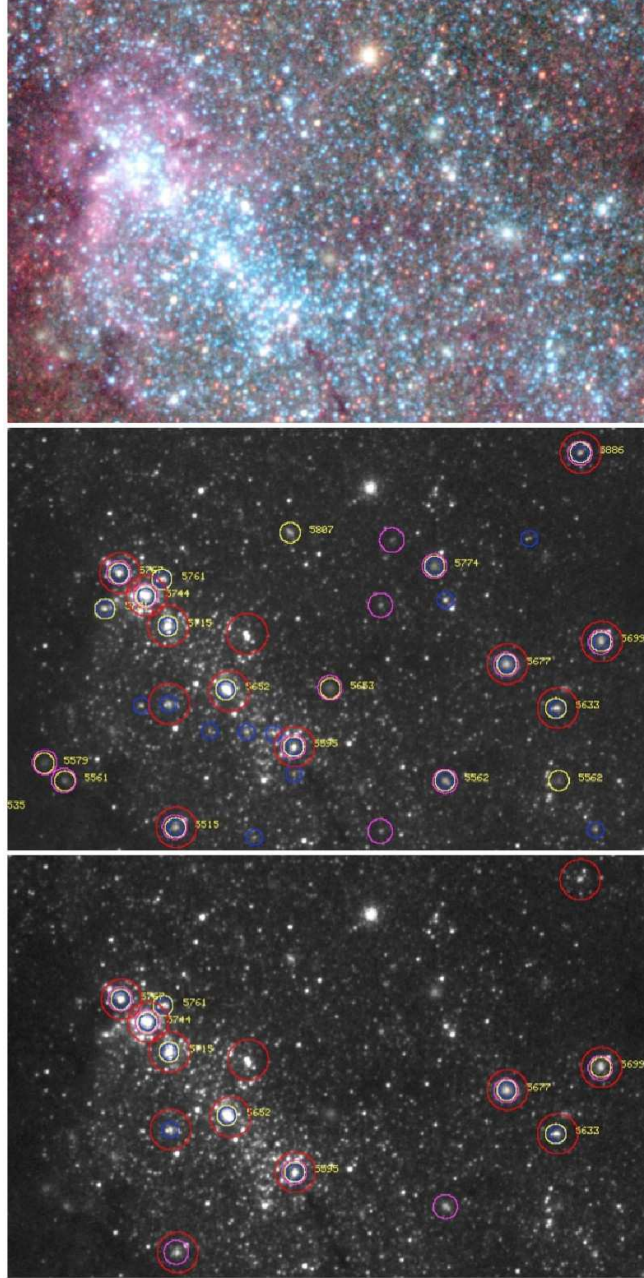


Fig. 2.— Comparison between catalogs discussed in Section 3. The top panel shows a color image of the region in M83 selected to make the comparison. The middle panel shows a comparison of the HLA-generated cluster catalog used in the present study (large red circles) with the other three catalogs (Chandar-automatic in blue, Chandar-manual in yellow, Bastian-hybrid in purple—see Chandar et al. 2013 for a similar figures and detailed description). The bottom panel imposes similar magnitude thresholds in order to facilitate a more equitable comparison.

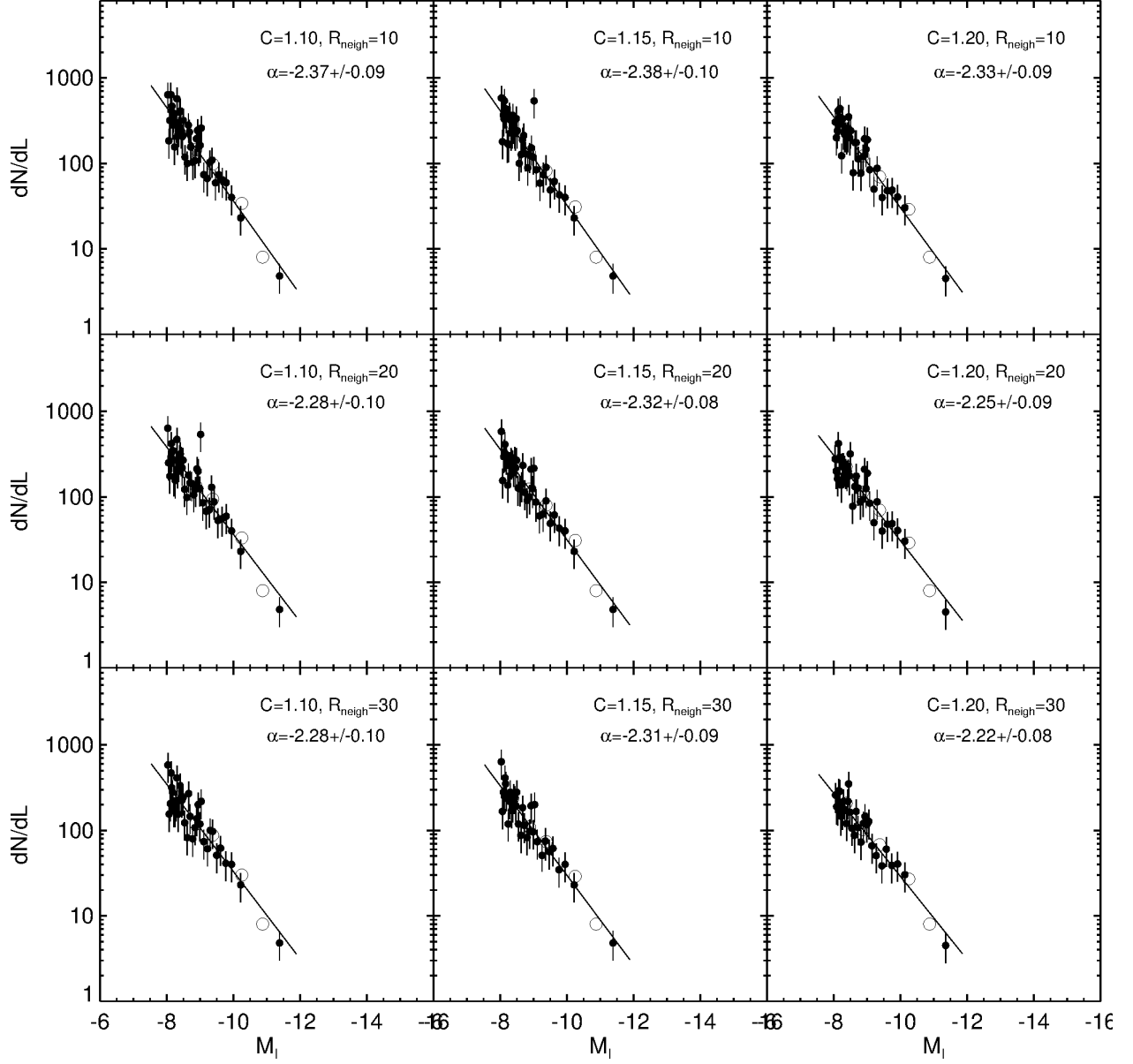


Fig. 3.— LFs for 3×3 grid of C and UNIQPOS parameters for M83. Open circles are for constant magnitude binning while filled circles are for constant number binning. See Section 3 for details.

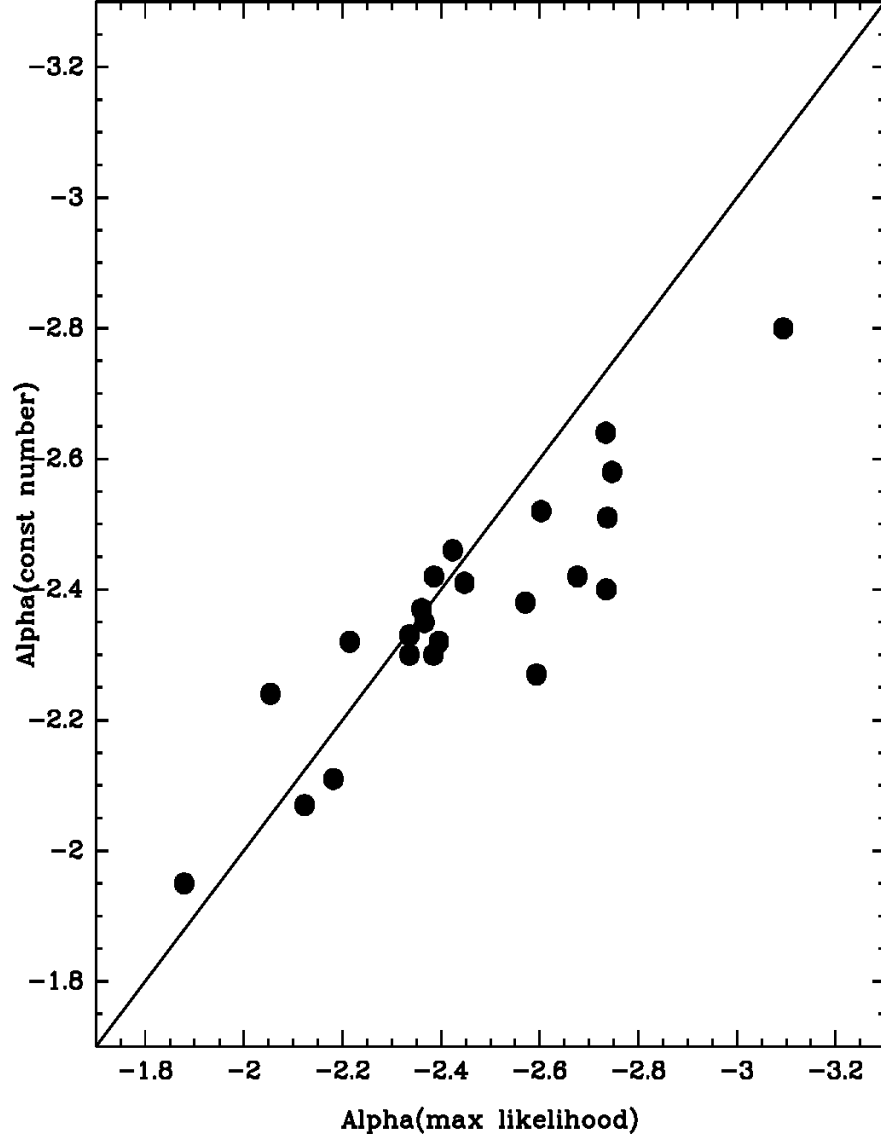


Fig. 4.— Comparison between values of α determined using the maximum likelihood and the constant number binning methods.

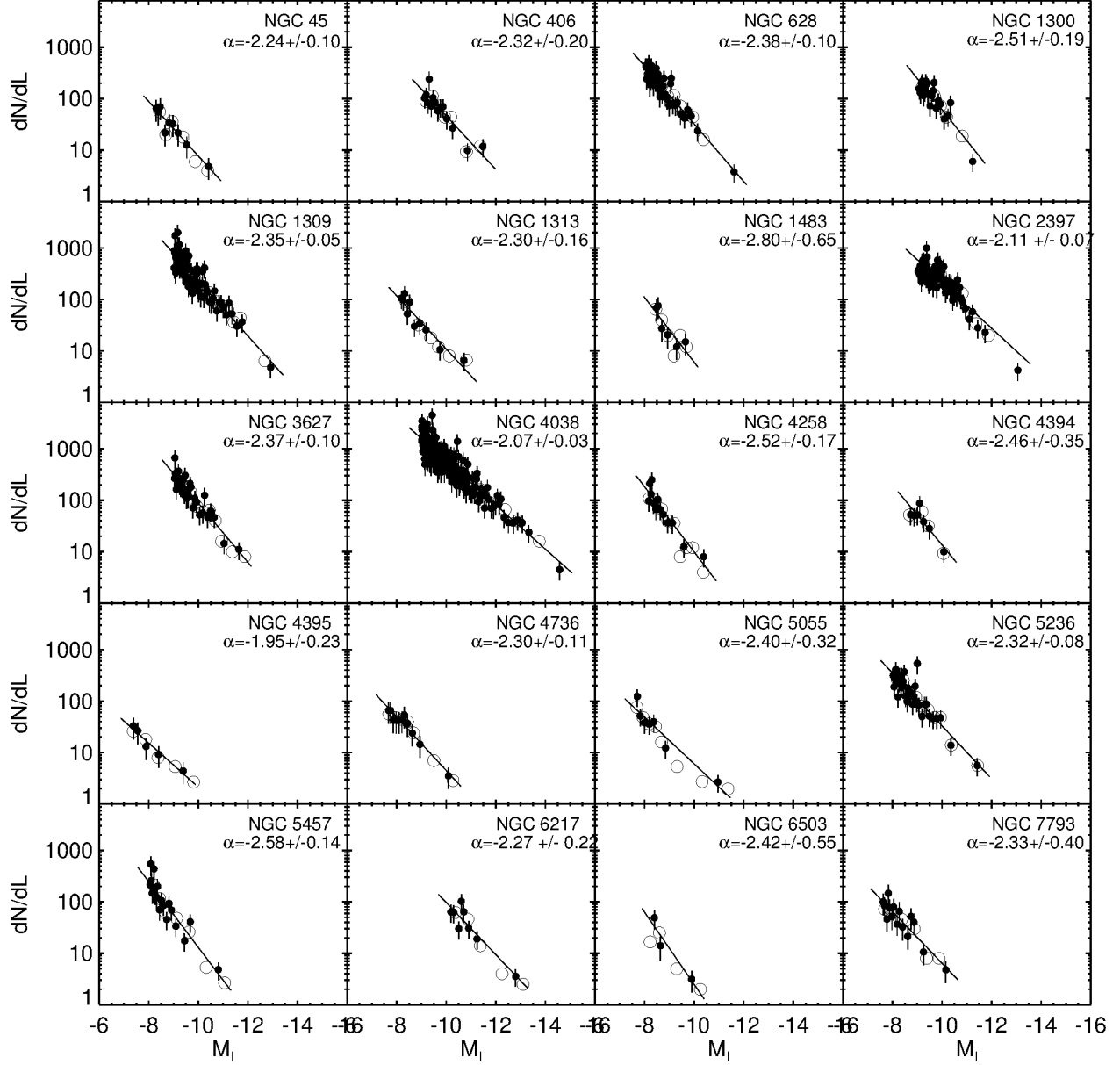


Fig. 5.— LFs for all 20 galaxies in our sample. Filled circles show the results using constant number per bin while open symbols show the results using constant magnitude bins. The values for α are for the constant number binning.

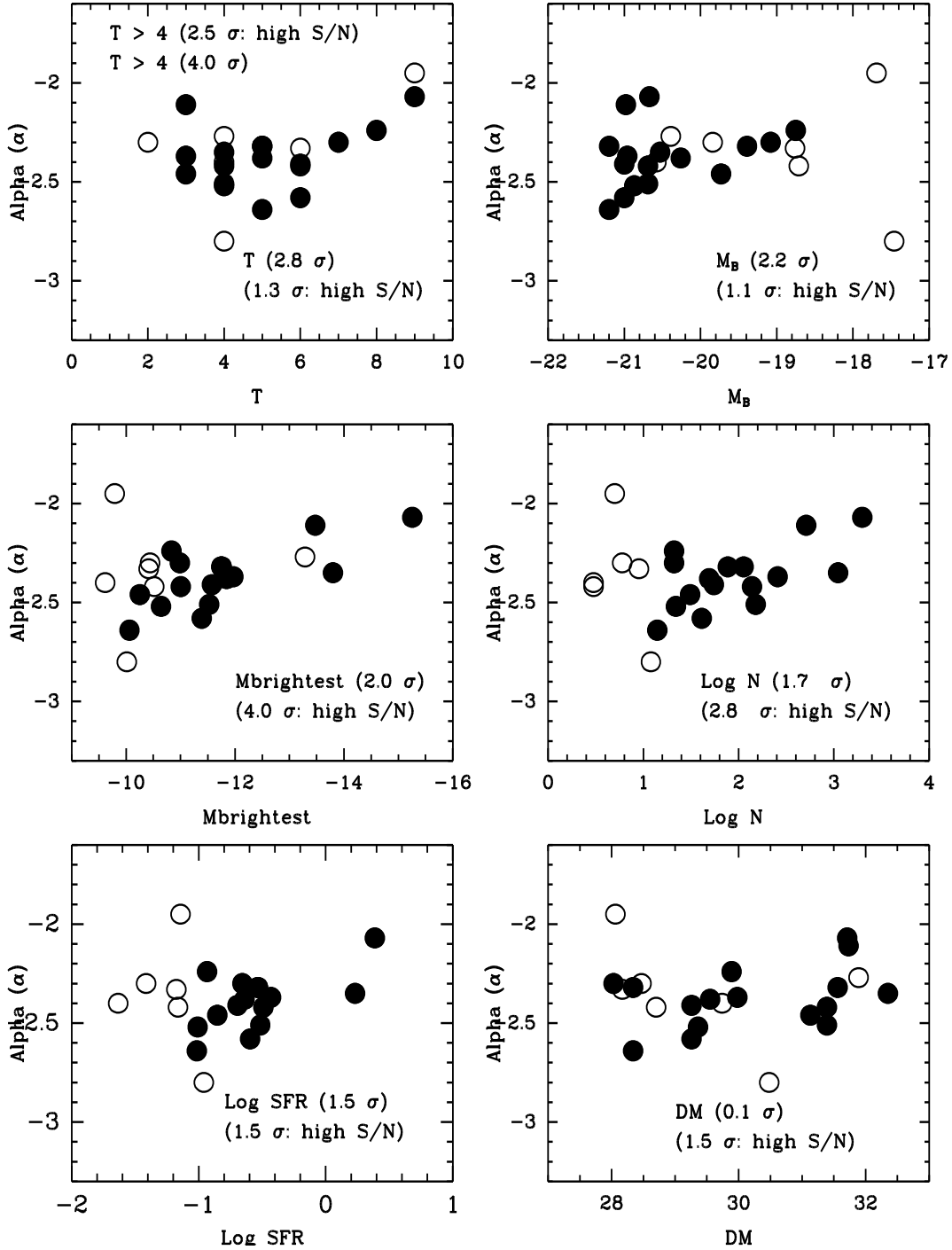


Fig. 6.— Correlation search using the α determinations from the constant number binning. Filled circles show the high S/N data (i.e., $\log N > 1.20$ for $M_I - 9$ mag limit) while open circles show the low S/N data. See Section 5.1 for details.

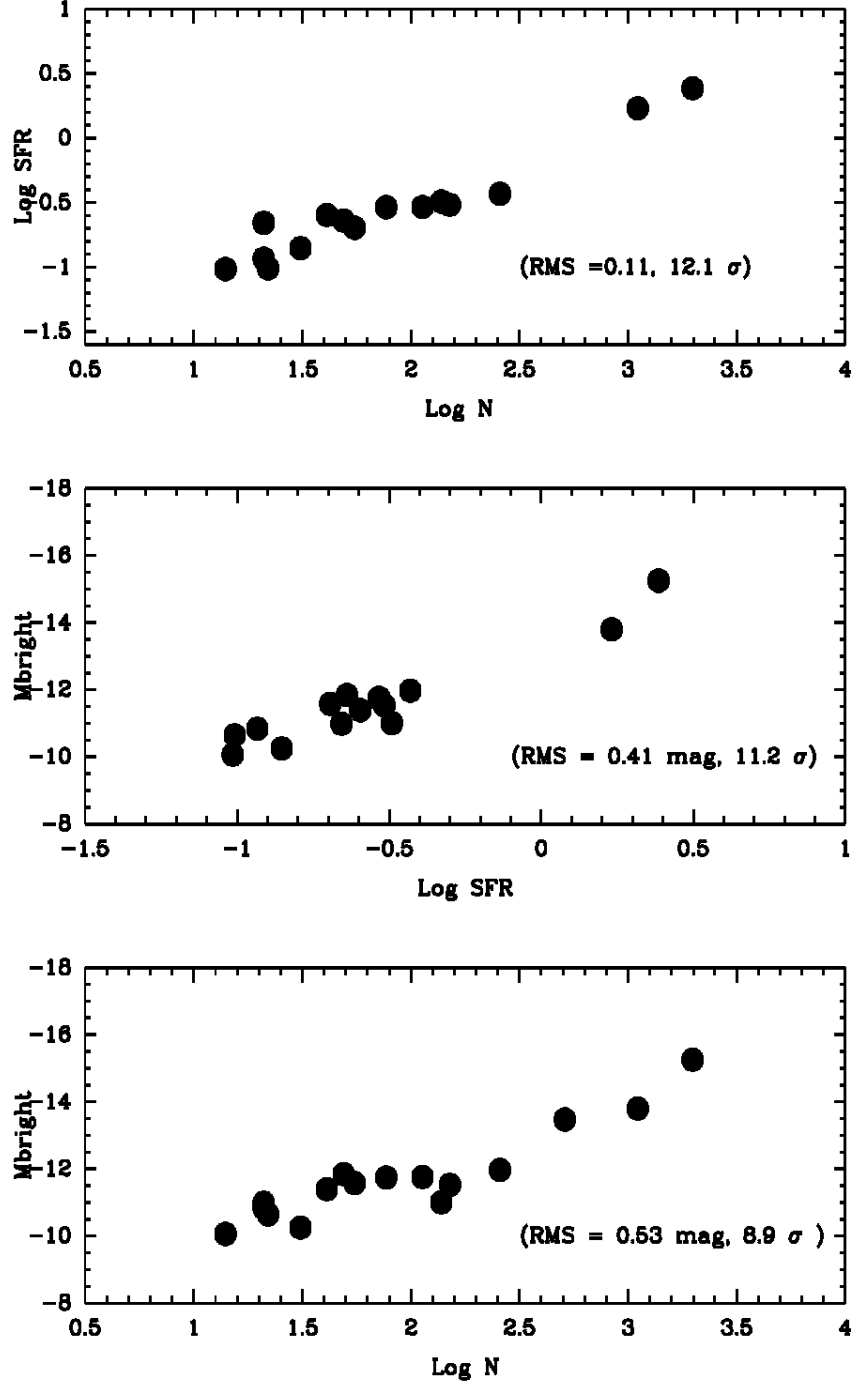


Fig. 7.— The correlations between $M_{\text{brightest}}$, $\log(N)$, and $\log(\text{SFR})$.

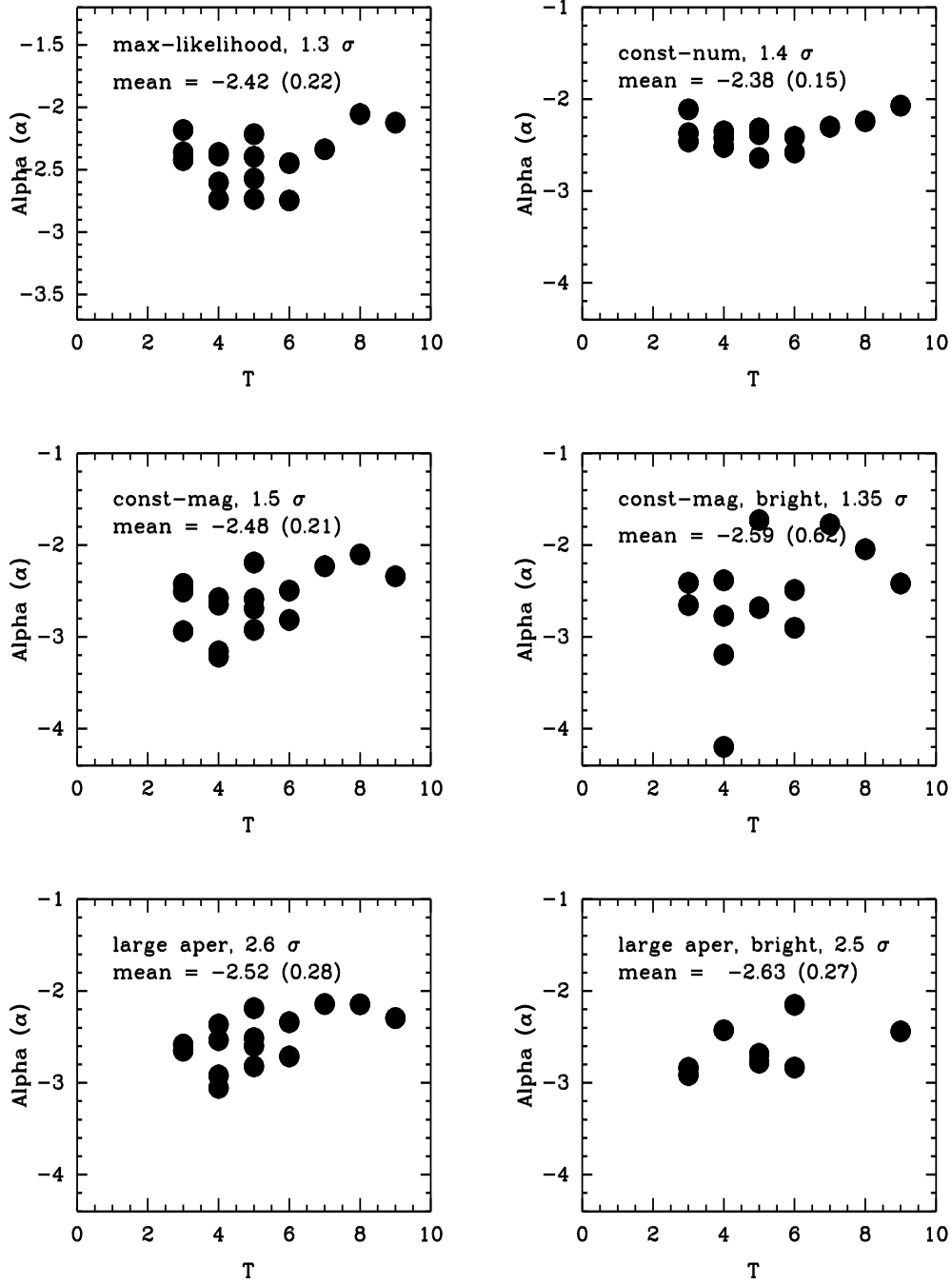


Fig. 8.— The correlations between Alpha (α) and Hubble type (T) using three different fitting methods (i.e., maximum-likelihood, constant number and constant magnitude); 7 pixels photometry (i.e., “large aper”); and the brighter part of the luminosity function (i.e., “bright”). See Section 3 for details.

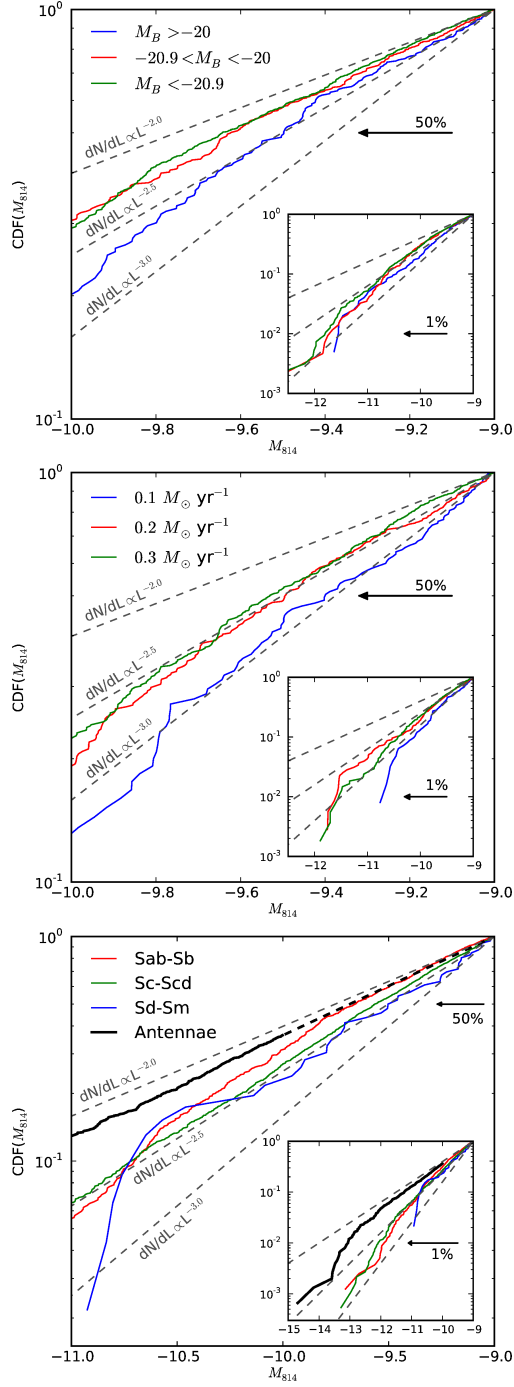


Fig. 9.— Each plot shows the Cumulative Distribution Functions (CDF) for the composite “supergalaxies” grouped by: top – absolute B magnitude, middle – SFR, bottom – Hubble type. Lines with constant values of $\alpha = -2$, -2.5 and -3 are included for comparison. See Section 5.2 for details.

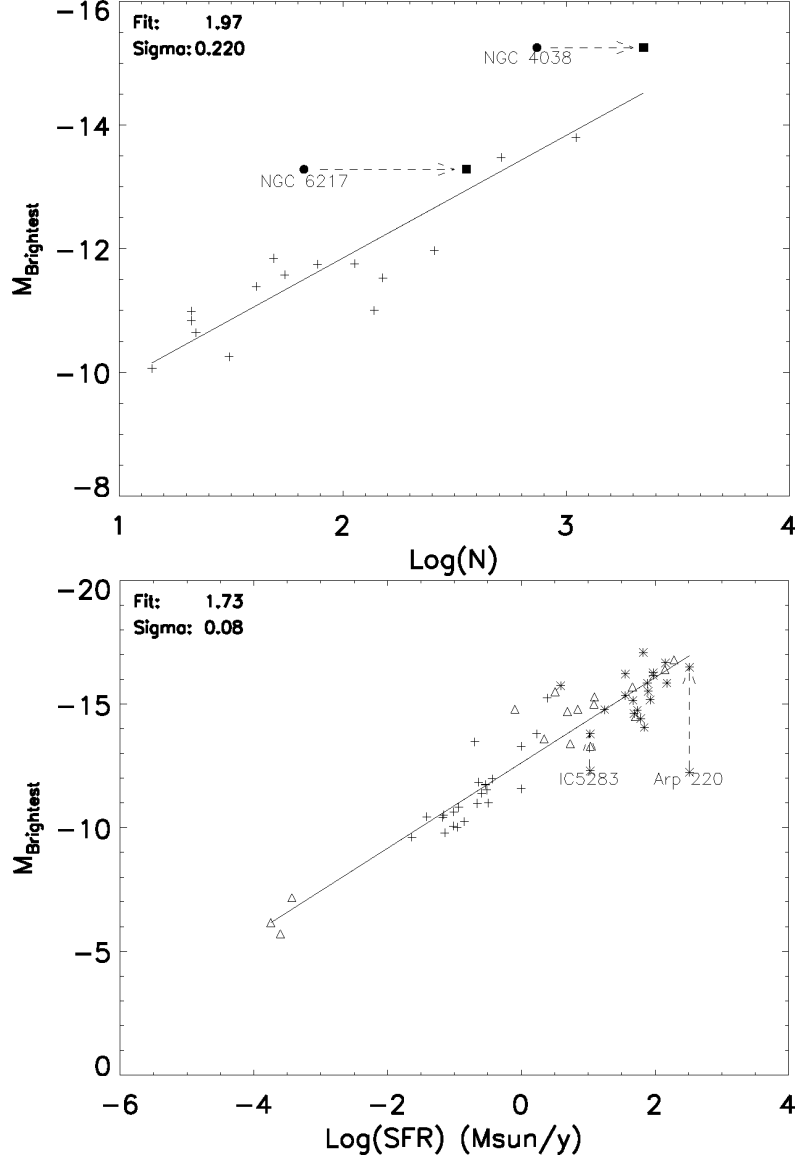


Fig. 10.— Log SFR vs. brightest cluster for the sample galaxies. The galaxies from the Vavilkin (2011) sample are marked with asterisks; the triangles are data from Bastian (2008). Data from the current sample are marked with a plus sign. See Section 5.3 for details.

Table 1. Basic Properties of Target Galaxies

Galaxy	Type	$m - M$	A_I	M_B	Proposal ID visit	Filters	SFR
NGC 45	SA(s)dm	29.89	0.040	−18.75	9774 03	<i>F336W</i> , F435W, F555W, F814W	0.1165
NGC 406	SA(s)c	31.56	0.046	−19.39	9395 03	F435W, F555W, F814W	0.2931
NGC 628	SA(s)c	29.55	0.135	−20.26	10402 23	<i>F336W</i> , F435W, F555W, F658N, F814W	0.2295
NGC 1300 (field 1)	SB(rs)bc	31.39	0.059	−20.69	10342 02	F658N, F814W	0.3051
NGC 1300 (field 2)	SB(rs)bc	31.39	0.059	−20.69	10342 04	F658N, F814W	0.3225
NGC 1309	SA(s)bc	32.35	0.077	−20.53	10497 10	F555W, F814W	1.7038
NGC 1313	SB(s)d	28.03	0.212	−19.08	9774 05	<i>F336W</i> , F435W, F555W, F814W	0.2205
NGC 1483	SB(s)bc	30.48	0.014	−17.46	9395 05	<i>F336W</i> , F435W, F555W, F658N, F814W	0.1098
NGC 2397	SB(s)b	31.73	0.398	−20.98	10498 02	F435W, F555W, F814W	...
NGC 3627	SAB(s)b	29.98	0.063	−20.96	11575 01	<i>F336W</i> , F435W, F555W, F658N, F814W	0.3709
NGC 4038	SB(s)mpec	31.71	0.090	−20.67	10188 10	<i>F336W</i> , F435W, F550M, F814W	2.4316
NGC 4258	SAB(s)bc	29.36	0.031	−20.87	9810 12	F435W, F555W, F814W	0.0981
NGC 4394	(R)SB(r)b	31.13	0.059	−19.73	10515 17	F475W, F814W	0.1402
NGC 4395	SA(s)m	28.06	0.033	−17.69	9774 0b	<i>F336W</i> , F435W, F555W, F814W	0.0719
NGC 4736	(R)SA(r)ab	28.47	0.034	−19.84	10402 07	<i>F336W</i> , F435W, F555W, F658N, F814W	0.0385
NGC 5055	SA(rs)bc	29.74	0.034	−20.58	10402 18	<i>F336W</i> , F435W, F555W, F606W, F814W	0.0232
NGC 5236 (field 1)	SAB(s)c	28.34	0.128	−21.20	9774 0f	<i>F336W</i> , F435W, F555W, F814W	0.2915
NGC 5236 (field 2)	SAB(s)c	28.34	0.128	−21.20	9774 0h	<i>F336W</i> , F435W, F555W, F814W	0.0967
NGC 5457 (field 1)	SAB(rs)cd	29.26	0.017	−21.00	9490 01	<i>F336W</i> , F435W, F555W, F814W	0.2541
NGC 5457 (field 2)	SAB(rs)cd	29.26	0.017	−21.00	9490 02	<i>F336W</i> , F435W, F555W, F814W	0.2021
NGC 6217	(R)SB(rs)bc	31.89	0.085	−20.39	11371 03	F658N, F814W	...
NGC 6503	SA(s)cd	28.70	0.062	−18.71	9293 11	F658N, F814W	0.0688
NGC 7793	SA(s)cd	28.17	0.038	−18.76	9774 0l	<i>F336W</i> , F435W, F555W, F814W	0.0667

Note. — All observations are from the ACS except F336W (in italics) which is from the WFPC2. F336W is included as reference information but not used in the paper.

Table 2. Summary of Cluster Catalogs

Galaxy	Brightness Limit, M_I	Concentration Index, C	Uniqpos R_{neighbor}	$M_{\text{brightest}}$	log N @ Brightness Limit	log N @ $M_I = -9$ Limit
NGC 45	-8.0	1.15	10	-10.83	1.79	1.32
NGC 406	-9.0	1.10	10	-11.75	2.05	2.05
NGC 628/M74	-8.0	1.15	10	-11.84	2.29	1.69
NGC 1300 (field 2)	-9.0	1.10	10	-11.00	2.13	2.13
NGC 1300 (field 1)	-9.0	1.10	10	-11.52	2.17	2.17
NGC 1309	-9.0	1.10	10	-13.80	3.04	3.04
NGC 1313	-8.0	1.25	25	-10.98	1.91	1.32
NGC 1483	-8.5	1.13	15	-10.01	1.61	1.07
NGC 2397	-9.0	1.10	10	-13.47	2.70	2.70
NGC 3627/M66	-9.0	1.10	10	-11.97	2.40	2.40
NGC 4038	-10.0	1.10	10	-15.25	2.86	...
NGC 4258	-8.0	1.15	10	-10.64	2.04	1.34
NGC 4394	-8.5	1.10	10	-10.25	1.74	1.49
NGC 4395	-7.0	1.30	30	-9.79	1.43	0.69
NGC 4736	-7.5	1.14	20	-10.44	1.79	0.77
NGC 5055/M63	-7.5	1.15	10	-9.61	1.68	0.47
NGC 5236 (field 1)/M83	-8.0	1.15	20	-11.74	2.42	1.88
NGC 5236 (field 2)/M83	-8.0	1.15	20	-10.06	1.88	1.14
NGC 5457 (field 1)/M101	-8.0	1.15	20	-11.38	2.29	1.60
NGC 5457 (field 2)/M101	-8.0	1.15	20	-11.57	2.30	1.74
NGC 6217	-10.0	1.10	10	-13.28	1.82	...
NGC 6503	-8.0	1.20	20	-10.51	1.39	0.47
NGC 7793	-7.5	1.24	30	-9.65	1.36	0.60

Table 3. Luminosity Function Fits

Galaxy	$\alpha_{\text{max-likelihood}}$	$\alpha_{\text{const-number}}$	Other α
NGC 45	-2.05 ± 0.19	-2.24 ± 0.10	$-1.94 \pm 0.28^{\text{a}}$
NGC 406	-2.21 ± 0.15	-2.32 ± 0.20	...
NGC 628	-2.57 ± 0.12	-2.38 ± 0.10	$-2.16 \pm 0.26^{\text{b}}$
NGC 1300 (field 1)	-2.74 ± 0.16	-2.51 ± 0.13	...
NGC 1300 (field 2)	-2.39 ± 0.18	-2.42 ± 0.18	...
NGC 1309	-2.37 ± 0.04	-2.35 ± 0.05	...
NGC 1313 (field 1)	-2.34 ± 0.18	-2.30 ± 0.16	$-2.10 \pm 0.12^{\text{b}}$, $-2.08 \pm 0.10^{\text{c}}$
NGC 1483	-3.09 ± 0.46	-2.80 ± 0.65	...
NGC 2397	-2.18 ± 0.06	-2.11 ± 0.07	...
NGC 3627	-2.36 ± 0.10	-2.37 ± 0.10	$-2.50 \pm 0.07^{\text{d}}$
NGC 4038	-2.12 ± 0.04	-2.07 ± 0.03	$-2.13 \pm 0.07^{\text{e}}$
NGC 4258	-2.60 ± 0.18	-2.52 ± 0.17	...
NGC 4394	-2.42 ± 0.32	-2.46 ± 0.35	...
NGC 4395	-1.88 ± 0.29	-1.95 ± 0.23	$-1.70 \pm 0.10^{\text{c}}$
NGC 4736	-2.38 ± 0.21	-2.30 ± 0.11	...
NGC 5055	-2.74 ± 0.32	-2.40 ± 0.32	...
NGC 5236 (field 1)	-2.40 ± 0.09	-2.32 ± 0.08	$-2.25 \pm 0.12^{\text{b}}$, $-2.38 \pm 0.11^{\text{c}}$
NGC 5236 (field 2)	-2.73 ± 0.26	-2.64 ± 0.29	...
NGC 5457 (field 1)	-2.75 ± 0.13	-2.58 ± 0.14	...
NGC 5457 (field 2)	-2.45 ± 0.11	-2.41 ± 0.12	...
NGC 6217	-2.59 ± 0.21	-2.27 ± 0.22	...
NGC 6503	-2.68 ± 0.41	-2.42 ± 0.55	...
NGC 7793	-2.34 ± 0.18	-2.33 ± 0.40	$-1.99 \pm 0.13^{\text{c}}$
Composite Galaxies			
SFR1 ^f	-2.89 ± 0.22
SFR2 ^f	-2.56 ± 0.09
SFR3 ^f	-1.95 ± 0.02
HT1 ^g	-2.30 ± 0.05
HT2 ^g	-2.43 ± 0.03

Table 3—Continued

Galaxy	$\alpha_{\text{max-likelihood}}$	$\alpha_{\text{const-number}}$	Other α
HT3 ^g	-2.17 ± 0.30
MB1 ^h	-2.52 ± 0.13
MB2 ^h	-2.41 ± 0.07
MB3 ^h	-2.36 ± 0.04

^aMora et al. 2007 – (B mag)

^bLarsen 2002 – (V mag)

^cMora et al. 2009 – (V mag)

^dDolphin & Kennicutt 2002 – V mag – NOTE: The original paper quotes a power law slope of -1.50 for a fit to the function $dN/d \log L$ rather than the more standard dN/dL used in this paper. A correction of -1 has therefore been added to their value to make the comparison.

^eWhitmore et al. 2010 – (V mag)

^fGalaxies Included – SFR1 = 4258, 4394, 4736, 5055, 6503, 45, 1483, 4395, 5236 (field 2), 7793; SFR2 = 1313, 406, 628, 5236 (field 1), 5457 (field 1), 5457 (field 2); SFR3 = 1300 (field 1), 1300 (field 2), 3627, 4038, 1309

^gGalaxies Included – HT1 = 4736, 4394, 3627, 2397; HT2 = 406, 5236 (field 1), 5236 (field 2), 628, 1483, 4258, 5055, 1309, 1300 (field 1), 1300 (field 2), 6217, 5457 (field 1), 5457 (field 2), 6503, 7793; HT3 = 1313, 45, 4395

^hGalaxies Included – MB1 = 1483, 4395, 6503, 7793, 1313, 406, 4394, 4736; MB2 = 628, 6217, 5055, 1300 (field 1), 1300 (field 2), 4258; MB3 = 2397, 3627, 5457 (field 1), 5457 (field 2), 5236 (field 1), 5236 (field 2)